Supplement of Biogeosciences, 21, 3305–3319, 2024
https://doi.org/10.5194/bg-21-3305-2024-supplement

Biogeosciences Open Access EGU

Supplement of

Distinguishing mature and immature trees allows estimating forest carbon uptake from stand structure

Samuel M. Fischer et al.

Correspondence to: Samuel M. Fischer (samuel.fischer@ufz.de)

Table of Contents

S1 Data availability by species

The table below displays basic information and data availability for each species in the inventory of 2014. The rows are sorted by the species' respective basal areas (including minor stems). The column "PFT" indicates the plant functional types the species were assigned to; the PFT numbers correspond to those provided in section S2.2. The column "Allometry data available" shows whether DBH-dependent data on allometric properties, such as tree height or crown length, were available. The column "Biomass equation available" indicates whether we found a suitable DBH biomass relationship in Chojnacky et al. (2014). Species not present in the inventory of 2014 were omitted.

The allometry dataset contained DBH values, heights, crown diameters, and crown lengths for individual trees. On average, the dataset contained 73 individuals per species covered in the dataset.

Note that when fitting allometric equations for plant functional types (PFTs), the species were weighted according to their share in the inventory (section S2.3). Hence, missing data are not expected to impact the fitted relationships significantly if the corresponding species have a small share of basal area in the inventory. Furthermore, the biomass equations were only used to approximate the relative share of each PFT in the inventory and estimate a single parameter per PFT based on this information (section .S2.4.5). Therefore, missing data are not expected to impact the model results significantly.

Species	Basal area in inventory $\left[\frac{\mathrm{m}^2}{\mathrm{ha}}\right]$	PFT	Shade tolerance	Allometry data available	Biomass equation available
Tilia amurensis	12.556	6	Shade tolerant	✓	✓
Pinus koraiensis	9.870	4	Midtolerant	✓	✓
Quercus mongolica	6.748	3	Light demanding	✓	✓
Fraxinus mandshurica	6.098	4	Midtolerant	✓	✓
Acer mono	2.552	6	Shade tolerant	✓	✓
Ulmus japonica	1.867	4	Midtolerant	✓	✓
Acer pseudo-sieboldianum	1.254	5	Shade tolerant	✓	✓
Populus ussuriensis	1.212	2	Light demanding	✓	✓
Tilia mandshurica	0.345	6	Shade tolerant	✓	✓
Maackia amurensis	0.285	4	Midtolerant	✓	–
Populus koreana	0.203	2	Light demanding	✓	✓
Acer barbinerve	0.199	5	Shade tolerant	–	–
Betula platyphylla	0.179	2	Light demanding	✓	✓
Corylus mandshurica	0.151	5	Shade tolerant	–	–

Species	Basal area in inventory $\left[\frac{\mathrm{m}^2}{\mathrm{ha}}\right]$	PFT	Shade tolerance	Allometry data available	Biomass equation available
Acer triflorum	0.120	6	Shade tolerant	✓	–
Acer tegmentosum	0.120	5	Shade tolerant	✓	–
Syringa reticulata	0.110	1	Light demanding	✓	–
Malus baccata	0.103	6	Shade tolerant	✓	–
Phellodendron amurense	0.100	2	Light demanding	✓	–
Acer mandshuricum	0.083	6	Shade tolerant	✓	–
Prunus padus	0.073	6	Shade tolerant	✓	–
Ulmus laciniata	0.068	4	Midtolerant	✓	–
Betula costata	0.053	2	Light demanding	✓	–
Populus davidiana	0.031	2	Light demanding	✓	–
Pyrus ussuriensis	0.026	2	Light demanding	✓	–
Abies nephrolepis	0.026	4	–	✓	–
Rhamnus ussuriensis	0.017	5	Shade tolerant	–	–
Cerasus maximowiczii	0.010	1	Light demanding	–	–
Acer ginnala	0.009	5	Shade tolerant	–	–
Sorbus alnifolia	0.006	5	Shade tolerant	✓	–
Philadelphus schrenkii	0.004	5	Shade tolerant	–	–
Rhamnus davurica	0.004	5	Shade tolerant	–	–
Crataegus maximowiczii	0.002	1	–	–	–
Euonymus pauciflorus	0.001	5	Shade tolerant	–	–
Euonymus alatus	0.001	5	Shade tolerant	–	–
Acanthopanax senticosus	0.000	5	Shade tolerant	–	–
Sambucus williamsii	0.000	1	Light demanding	–	–
Lonicera chrysantha	0.000	5	–	–	–
Viburnum sargenti	0.000	5	Shade tolerant	–	–
Actinidia kolomikta	0.000	5	–	–	–
Viburnum bureiaeticum	0.000	5	Shade tolerant	–	–
Rhamnus diamantiaca	0.000	5	Shade tolerant	–	–
Euonymus macropterus	0.000	5	Shade tolerant	–	–
Vitis amurensis	0.000	5	–	–	–
Aralia elata	0.000	5	Shade tolerant	–	–

Species	Basal area in inventory $\left[\frac{\mathrm{m}^2}{\mathrm{ha}}\right]$	PFT	Shade tolerance	Allometry data available	Biomass equation available
Deutzia amurensis	0.000	5	–	–	–
Sorbaria sorbifolia	0.000	4	–	–	–

S2 Parameterization of the forest model FORMIND

The forest model FORMIND is described in detail by Bohn et al. (2014) and Fischer et al. (2016). Below we focus on those aspects of the model that deviate from this description, and we provide details about the parameter choice and model fitting procedure. We based our analysis on forest inventory data from an old-growth temperate forest in the Changbaishan National Nature Reserve in northeastern China. The surveyed area consists of $25\,\mathrm{ha}$ of conifer/broad-leaf mixed forest with 47 species, a total biomass of $302\,{}^{\mathrm{t\,ODM}}/_{\mathrm{ha}}$ (Piponiot et al., 2022). The inventory data contain the position, diameter at breast height (DBH) and species of each tree with $\mathrm{DBH} \geq 1\mathrm{cm}$ for the census years 2004, 2009, and 2014. Each tree is uniquely identified with an ID number. For trees that had multiple stems at breast height, we focused on the main stem (maximal DBH) in our analysis and we disregarded minor stems.

Below we provide an overview of the parameterization procedure before describing each step in detail.

Overview

We started by assigning species to PFTs, which aggregate species dependent on their shade tolerance and sizes (section S2.2). Where no shade tolerance data were available, we assigned species to a PFT based on the light demand of their saplings and their median observed DBH increment. Next, we derived environmental parameters from the literature and public data sets (section S2.10).

To incorporate species traits and allometric relationships into the model, we computed mean trait values / allometries for each PFT based on independent species-specific data sets or the literature, weighting the species according to their basal area share in the inventory. For size-dependent traits / allometries, we fitted simple functions mapping the DBH to the corresponding trait value. We considered the following DBH-dependent traits: Tree height (section S2.3.1), crown length (section S2.3.2), crown diameter (section S2.3.3), stem from factor (section S2.3.4), and LAI (section S2.4.3). Furthermore, we considered the following constant traits: maximal DBH (section S2.4.1), wood density (section S2.4.2), light extinction coefficient (section S2.4.4), and mean stem biomass proportion (mean taken over DBH values; section S2.4.5).

To parameterize the modelled processes, we used a combination of approaches. Where possible, we derived parameters by comparing inventory data from two consecutive censuses. This applied to the parameters of the optimal potential growth of trees (section S2.7.1) and tree mortality (section S2.9). Some further parameters could be derived by considering the light climate that FORMIND obtains for the forest state observed in the inventory. That way, we could estimate the maximal incident radiation of trees in the inventory (section S2.7.2) and constrain the carbon use efficiency (CUE) of trees (section S2.7.4). The remaining process-related parameters were determined by fitting the results from dynamic model simulations to the observed inventory data. With this approach, we obtained the parameters for the seed influx (section S2.5), ingrowth of saplings (section S2.6), photosynthesis (section S2.7.3), carbon losses other than maintenance respiration (section S2.7.4), as well as another parameter controlling the optimal growth of trees (section S2.7.1).

To fit the model to the inventory data by optimizing the latter parameters, we used a likelihood-based approach, maximizing the likelihood with which the collected inventory data are observed according to the model (section S2.11). This method has the advantage that it can be applied on small scales (here: $0.04\,\mathrm{ha}$), where forest data are highly stochastic and can have strongly skewed distributions. The approach fits the model not only to spatially aggregated forest attributes but considers their entire distribution. That is, it seeks to reproduce the frequency of each possible forest state, including uncommon or extreme states. By considering the complete state distribution, more information is used in the fitting stage, and parameters can be estimated with higher precision and accuracy.

Though we largely applied the same FORMIND version used in previous studies (Fischer et al., 2016), we also adjusted some submodels to achieve higher realism and to assert that fitted parameters do not lead to unreasonable model behaviour. We made the following procedural adjustments:

Individual-specific size limits (section S2.4.1): We allowed each individual tree to have a different DBH limit. That way, we could account for (1) different size limits of the species within the PFTs and (2) heterogeneity in local conditions constraining tree height. Without individual-specific size limits, all mature trees in a PFT would have had the same size, potentially introducing model artifacts to the relationships between forest structure and tree maturity and hence forest productivity.

Ingrowth (section S2.6): Rather than using sharp light thresholds to decide whether seeds can establish to saplings, we used sigmoid curves that allow a small fraction of seeds to establish even under unfavourable conditions. This approach avoids sudden strong changes in ingrowth dynamics, potentially leading to greater heterogeneity in forest patches.

Optimal DBH increment (section S2.7.1): We estimated the optimal growth of trees as a certain quantile of the DBH increment distribution. This approach is more robust than simply considering maximal observed DBH increments, as it is insensitive to outliers and avoids the statistical bias that could occur if the tree size distribution is not uniform.

Reference light conditions (section S2.7.2): We assumed that the maximal DBH increments observed in the inventory were achieved under shaded conditions for small trees. In earlier parameterizations of FORMIND, it was typically assumed that the fastest-growing trees in the inventory were not shaded, irrespective of their size. For the Changbaishan forest, this was not in line with the light climate that FORMIND estimated based on the inventory data.

CUE under optimal conditions (section S2.7.4) / size-dependent biomass allocation (section S2.7.5): We introduced a submodel for the optimal CUE of trees and used this along with biomass data to derive DBH-dependent stem and crown biomass proportions and to scale the light response curve (c.f. the introduction of section S2.7). Without this approach, GPP and respiration would have had to be parameterized independently of one antother, making it likely (sometimes inevitable) to run into situations where for some trees either (1) the parameterized GPP does not suffice for the biomass increment observed in the inventory, resulting in zero-estimates for the maintenance respiration of these trees or (2) the parameterized GPP exceeds the observed biomass increment by orders of magnitude, resulting in maintenance respiration estimates so high that even moderately shaded trees cannot satisfy their respiratory needs and die. These situations cannot occur if the optimal CUE is fixed to reasonable values.

Defoliation (section S2.7.6): We created a new submodel for stress situations in which trees' maintenance respiration exceeds their GPP. In the new model, trees loose leaves and biomass until their remaining respiratory needs can be satisfied. As the loss of leaves leads to a further decline of GPP, stress can result in a feedback loop leading to tree death. Hence, the defoliation mechanism constrains the forest density in a mechanistic manner. The previous approach to model space competition was based on stochastic crowding mortality and would have capped the forest density even if all trees had a positive NPP and thus growth potential. By linking the maximal forest density to productivity and respiration, the defoliation approach also helped to obtain realistic parameters for the corresponding submodels.

After providing an overview of the parameterization procedure, we list all parameterization details required to reproduce the study results.

S2.1 Time step and simulation area

We ran the model using a yearly time step. We simulated a square-shaped forest area of one hectare, subdivided into 25 patches of $20\mathrm{m} \times 20\mathrm{m}$, in which light competition occurs. Plants in different patches interact via tree falling only. For this interaction, we assume torus boundary conditions to minimize boundary effects.

S2.2 Classification of species to plant functional types (PFTs)

We assigned the 47 tree species into 6 plant functional types (PFTs) according to their shade tolerance and their maximal height. In addition, we considered the species Mongolian Oak (*Quercus mongolica*) individually, as it had a unique DBH distribution in the forest, making it difficult to assign it to other PFTs without major information loss. We considered the following 6 PFTs:

1. Small shade intolerant species (pioneers with maximal diameter at breast height (DBH) below $30\mathrm{cm}$).
2. Large shade intolerant species 1 (pioneers with maximal DBH exceeding $30\mathrm{cm}$).
3. Large shade intolerant species 2 (Mongolian oak).
4. Large mid-tolerant species (intermediate species with maximal DBH exceeding $30\mathrm{cm}$).
5. Small shade tolerant species (climax species with maximal DBH below $30\mathrm{cm}$).
6. Large shade tolerant species (climax species with maximal DBH exceeding $30\mathrm{cm}$).

We did not consider a PFT of small mid-tolerant species, because there were no mid-tolerant species with maximal DBH below $30\mathrm{cm}$.

Classification of species with unknown shade tolerance class

We assigned species for which shade tolerance classification data were not readily available to the PFTs via a likelihood-based cluster analysis. For this analysis, we determined the median DBH change after 5 years for each species' individuals observed in the inventory. We used this value along with numerical shade tolerance data (Niinemets and Valladares, 2006; Wang et al., 2010), indicating the fraction of sunlight that a sapling requires to grow, as covariates. A shade tolerance value of 1 corresponds to a light requirement of $> 50\%$ of the full sunlight; 2 to 25%–50%; 3 to 10%–25%; 4 to 5%–10%; 5 to 2%–5%.

We assumed that the covariates follow a multivariate normal distribution $\mathcal{N}(\mu_i, \Sigma_i)$ for each shade tolerance class i. We estimated the means μ_i and covariance matrices Σ_i using the method of moments. For each shade tolerance group i, we

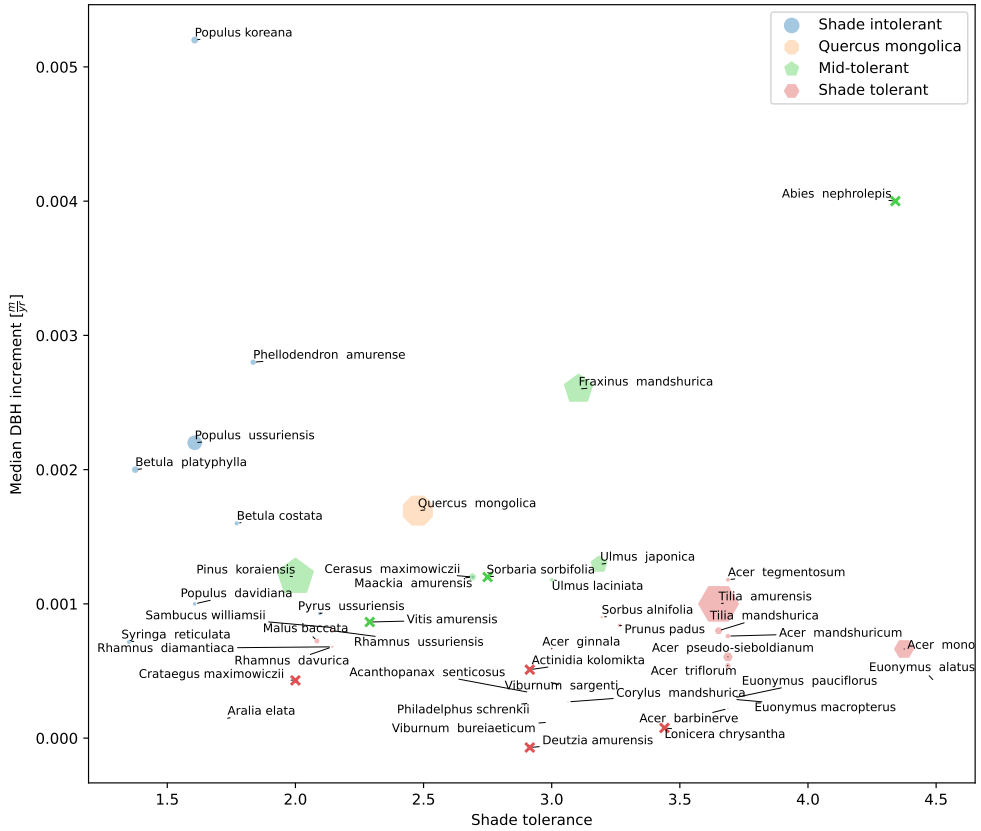

Figure S1. Assignment of species to PFTs with unknown shade tolerance based on a cluster analysis. Each colour corresponds to a shade tolerance type: shade intolerant (blue), mid-tolerant (green), shade tolerant (red). *Quercus mongolica* is drawn in a separate colour (orange), as it is a PFT on its own. Circles indicate species with a known shade tolerance type. The size of the circles correspond to the respective species' basal area in the inventory. Crosses depict species for which the shade tolerance type was assigned via the cluster analysis. The shade tolerance values indicate the fraction of sunlight that a sapling of the respective species requires to grow. Here, 1 corresponds to a light requirement of $> 50\%$ of the full sunlight; 2: 25%–50%; 3: 10%–25%; 4: 5%–10%; 5: 2%–5%.

determined the mean values μ_{ij} of the covariates j and covariances $\Sigma_{ij_1j_2}$ between covariate j_1 and j_2. We assigned each species s with unknown shade tolerance type to the class for which the likelihood based on the derived distributions was maximized. That is, with x_s being the covariate vector of species s and $f_{\mathcal{N}}$ the density function of the two-dimensional multivariate normal distribution, we set

$$\text{class}(s) = \underset{\text{classes } i}{\text{argmax}}\, f_{\mathcal{N}}(x_j; \mu_i, \Sigma_i). \tag{S1}$$

Fig. S1 depicts the classification of the species into shade tolerance classes.

S2.3 Allometric relationships

We determined allometric relationships for the six PFTs based on allometry data for the individual species. Specifically, we estimated the relationships between DBH and the geometric properties tree height, crown length, and crown radius, respectively. Let p be the index of a geometric property, i the considered PFT, θ_{pi} a parameter vector and x_{pi} the value of allometric property p for PFT i, d be the DBH and $g_p : \mathbb{R}_+ \to \mathbb{R}_+$ an injective function. Then we set

$$x_{pi} = g_p(d; \theta_{pi}). \tag{S2}$$

To estimate the parameter vectors θ_{pi}, we used a dataset containing tuples of tree DBH and tree height, crown length, and crown radius for several species. As we desired to find the allometric relationships that best represent the considered forest in Changbaishan, we weighted the data according to the frequency of trees with similar species and DBH in the inventory (see subsection S6.1). Then we fitted the parameters θ_{pi} based on the weighted likelihood, assuming that the data were subject to a normally distributed error with constant variance σ_{pi}^2:

$$X_{pi} \sim \mathcal{N}\big(g_p(d; \theta_{pi}), \sigma_{pi}^2\big), \tag{S3}$$

where X_{pi} denotes the observed geometry values. This reduces to a weighted least squares method. That is, the objective function can be expressed as

$$\bar{\ell}(\theta_{pi}) = -\sum_{k \in \mathcal{A}_i} \left(x_{pik} - g_p(d_k; \theta_{pi})\right)^2 w_k, \tag{S4}$$

where $\mathcal{A}_i$ is the set of entries in the allometry dataset corresponding to trees of PFT i, x_{pk} is the observed value for the geometric property p in entry k, d_k is the corresponding DBH value, and w_k is the weight. To maximize the likelihood, we used a Newton-Raphson-type trust region approach (Conn et al., 2000) as provided in the Python library Scipy (Jones et al., 2001).

For some species, no allometry data were available even though they were present in the inventory. Due to the lack of data, these species were not taken into account when fitting the allometric relationships. However, they were responsible for only a small share ($4\,\%$) of the basal area in the inventory (cf. section S1), so that their impact on the fitted relationships would have been small and we expect the lack of data not to bias the results significantly.

	Unit	Small shade intolerant	Large shade intolerant 1	Large shade intolerant 2	Large mid-tolerant	Small shade tolerant	Large shade tolerant
$\theta_{\text{height},i,0}$	$\frac{\text{m}}{\text{m}}$	127.81	198.06	174.00	143.19	167.82	129.98
$\theta_{\text{height},i,1}$	m	29.25	30.59	31.22	36.75	19.87	38.92
$\theta_{\text{crown-l},i}$	$\frac{\text{m}}{\text{m}}$	0.35	0.33	0.36	0.36	0.37	0.35
$\theta_{\text{crown-d},i,0}$	$\frac{\text{m}}{\text{m}^{\theta_{\text{crown-d},i,1}}}$	12.01	13.35	14.34	11.27	15.72	12.72
$\theta_{\text{crown-d},i,1}$	1	0.49	0.63	0.59	0.52	0.48	0.48

Table S2. Parameter values for allometric relationships.

S2.3.1 Height

For the relationship between DBH and tree height, we used the model

$$g_{\text{height}}(d;\theta_{\text{height},i}) = \frac{\theta_{\text{height},i,0}\theta_{\text{height},i,1}d}{d\cdot\theta_{\text{height},i,0}+\theta_{\text{height},i,1}}, \tag{S5}$$

where $\theta_{\text{height},i,0}$ is the initial slope of g_{height} and $\theta_{\text{height},i,1}$ is the height asymptote. The fitted parameter values are displayed in Table S2; the fitted curves are shown in Fig. S2a..

S2.3.2 Crown length

We used a linear relationship to model the relationship between tree height and crown length:

$$\tilde{g}_{\text{crown-l}}(h;\theta_{\text{crown-l},i}) = \theta_{\text{crown-l},i}\cdot h, \tag{S6}$$

where h is the tree height. With equation (S5), equation (S6) can also be expressed as a function of the DBH:

$$g_{\text{crown-l}}(d;\theta_{\text{height},i},\theta_{\text{crown-l},i}) = \theta_{\text{crown-l},i}\cdot g_{\text{height}}(d;\theta_{\text{height},i}). \tag{S7}$$

The fitted parameter values are displayed in Table S2; the fitted curves are depicted in Fig. S2b.

S2.3.3 (Maximal) crown diameter

For the relationship between DBH and crown diameter, we used a power-law model:

$$g_{\text{crown-d}}(d; \theta_{\text{crown-d},i}) = \theta_{\text{crown-d},0} \cdot d^{\theta_{\text{crown-d},1}}, \tag{S8}$$

where $\theta_{\text{crown-d},0}$ is the scaling factor and $\theta_{\text{crown-d},1}$ is the exponent. The fitted parameter values are displayed in Table S2 and the fitted curves in Fig. S2c.

Typically, the crown diameter of trees varies with height, and the available allometry data represent *maximal* crown diameters. In this parameterization of FORMIND, however, crowns are assumed to have cylindrical shapes, with diameters constant along the vertical axis. Hence, using the observed maximal crown diameters as diameters of the cylindrical shapes used in the model would lead to an overestimation of crown volumes and, as a result, the LAI. To correct for this potential bias, we assumed that the trees from which the data were taken had crowns shaped like ellipsoids, rotationally symmetric around the vertical axis. A cylinder with the same volume and height as this ellipsoid must have a diameter scaled by factor $\sqrt{\frac{2}{3}}$ as compared to the length of the horizontal semi-axis of the ellipsoid. Hence, we parameterized the model with the scaled DBH-crown-diameter relationship

$$g_{\text{crown-d}}(d; \theta_{\text{crown-d},i}) = \sqrt{\frac{2}{3}}\theta_{\text{crown-d},0} \cdot d^{\theta_{\text{crown-d},1}}. \tag{S9}$$

S2.3.4 Stem volume and form factor

To compute the stem volume $V_{\text{stem},i}$, we used the formula

$$V_{\text{stem},i}(d) = \frac{\pi}{4} d^2 g_{\text{height}}(d; \theta_{\text{height},i}) \nu_i(d), \tag{S10}$$

where d is the DBH, $g_{\text{height}}(d; \theta_{\text{height},i})$ is the height (see equation (S5)), and $\nu_i(d)$ is a DBH- and PFT-dependent form factor. A form factor $\nu_i(d) = 1$ corresponds to a cylindrical stem shape, $\nu_i(d) = \frac{1}{3}$ to a cone, $\nu_i(d) \in \left(1, \frac{1}{3}\right)$ to a convex cone-like shape, and $\nu_i(d) \in \left(1, \frac{1}{3}\right)$ to a concave cone-like shape of the stem. In line with earlier parameterizations of FORMIND (Dislich et al., 2009), we chose

$$\nu_i(d) = \theta_{\text{form},i,0} d^{\theta_{\text{form},i,1}} \tag{S11}$$

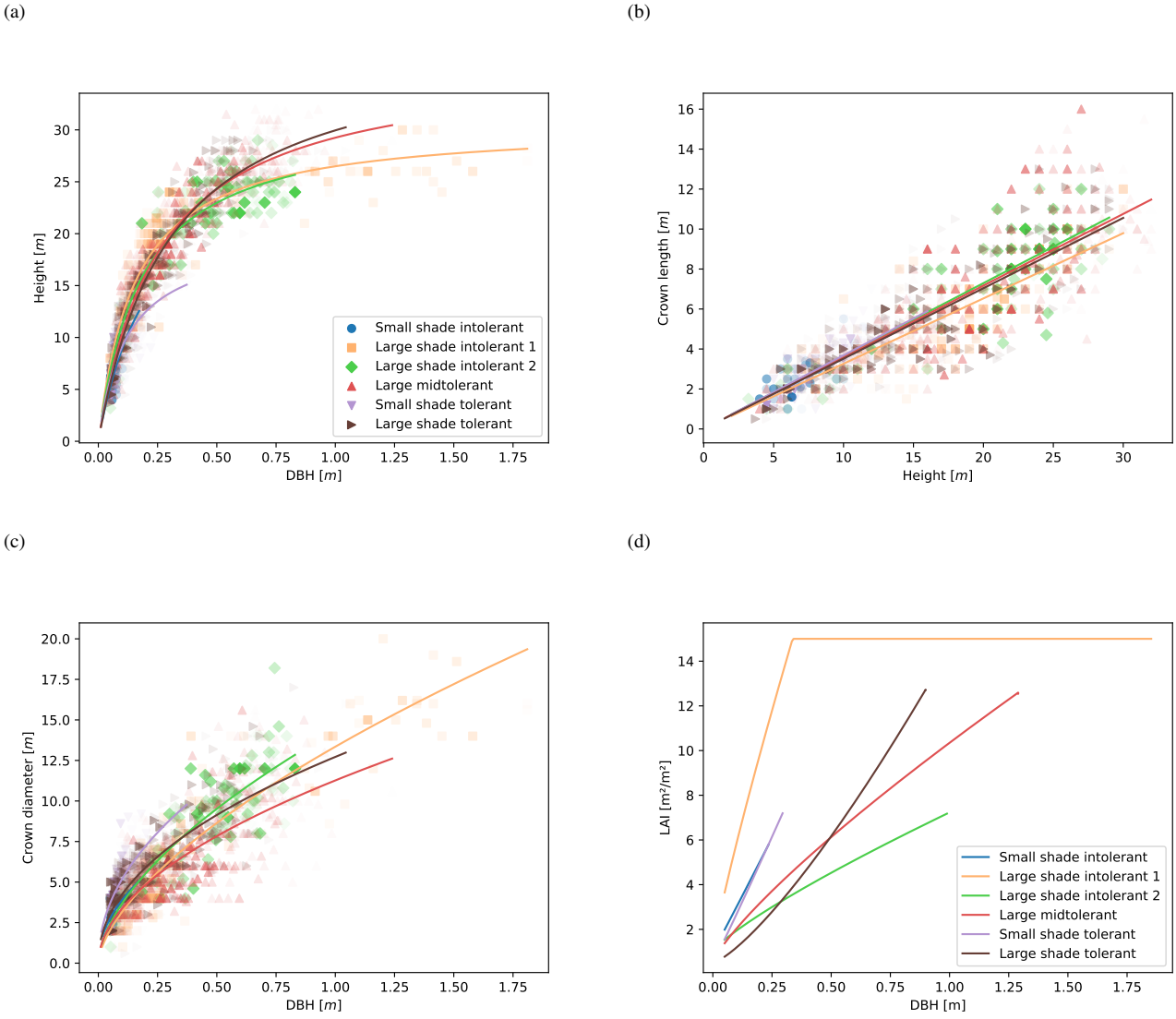

Figure S2. Size-dependent plant traits. The circles depict data points from the allometry dataset; their opacity shows their weight. Each colour corresponds to a different PFT: small shade intolerant (blue), large shade intolerant 1 (orange) large shade intolerant 2 (green), large mid-tolerant (red), small shade tolerant (purple), large shade tolerant (brown).

with $\theta_{\mathrm{form},i,0} = 0.336\,\mathrm{m}^{-\theta_{\mathrm{form},i,1}}$ and $\theta_{\mathrm{form},i,1} = -0.18$ for all PFTs i.

S2.4 Plant traits

Besides geometric relationships, the FORMIND model requires information about the maximal size of trees, their wood density, and their leaf area index (LAI).

S2.4.1 Maximal DBH

We assumed that each tree t has its own site-dependent maximal DBH $d_t^{\max}$. As this value may depend on the tree's species, which is neglected when species are summarized to PFTs, we constructed the distribution of maximal heights based on each species' maximal DBH and the species' frequency in the inventory. Below we provide a detailed description of our approach.

Let s be a species and $\mathcal{A}_s$ and $\mathcal{I}_s$ the subsets of the allometry and inventory dataset, respectively, that correspond to species s. We determine the maximal DBH of species s based on the maximal DBH observed in the allometry dataset and the 99.5th percentile of the inventory:

$$\bar{d}_s^{\max} = \max\left\{ F^{-1}_{\{d_k, k\in\mathcal{A}_s\}}(0.995), \max_{t\in\mathcal{I}_s} d_t \right\}, \tag{S12}$$

where $F_{\cdot}^{-1}(\cdot)$ is the observed percentile function.

There were some cases in which the maximal DBH from the inventory dataset was more than 10% lower than the corresponding maximum from the allometry dataset (here: $10\% \mathrel{\hat{=}} 15\,\mathrm{cm}$ difference). This may indicate that for these species, local conditions are unfavourable, which in turn should be reflected in the parameterization. In cases where we had enough (more than 1000) trees in the inventory to suggest that the maximal DBHs in the inventory coincide with the maximal DBH reachable the study site, we therefore used the value $F^{-1}_{\{d_k, k\in\mathcal{A}_s\}}(0.995)/0.9$. These cases are shown in Table S3.

We determined the frequency of each species in the inventory based on its total basal area. Based on this, we constructed a discrete probability distribution for the maximal tree height of a tree t. Let $\mathcal{S}_i$ be the species belonging to PFT i. We obtained the following probability mass function for the maximal height of a tree of PFT i:

$$p_i^{\max}(d) = \frac{\sum_{s\in\mathcal{S}_i} \mathrm{I}_{\{\bar{d}_s^{\max}\}}(d) w_s}{\sum_{s\in\mathcal{S}_i} w_s} \tag{S13}$$

Species	Number of trees with DBH $\geq 5\,\mathrm{cm}$ in the inventory	Maximal diameter estimated from the inventory data [m]	Maximal diameter estimated from the allometry data [m]	Value used in the model [m]
Acer mono	2469	0.38	0.61	0.43
Acer pseudo-sieboldianum	1722	0.20	0.37	0.23
Pinus koraiensis	2236	0.79	0.98	0.88
Tilia amurensis	2115	0.76	1.04	0.85

Table S3. Maximal DBH values for species where the estimates from the inventory and the allometry data deviate strongly.

with

$$w_s = \sum_{t \in \mathcal{I}_s} d_t^2 \tag{S14}$$

and the indicator function $\mathrm{I}_{\{X\}}(x)$, which is 1 id $x \in X$ and 0 otherwise.

Since even trees of the same species may have different site-dependent growth limits and to reduce a potential model artifact arising from drawing the maximal DBHs from discrete distributions, we constructed continuous distributions for the maximal diameters by blurring the distribution below the maximal DBH values $\bar{d}_s^{\max}$. That way, we obtained a continuous distribution with probability density function

$$f_i^{\max}(d) = c \sum_{s \in \mathcal{S}_i} \mathrm{I}_{\left[(1-\beta)\bar{d}_s^{\max}, \bar{d}_s^{\max}\right]}(d) \frac{w_s}{2\beta \bar{d}_s^{\max}}, \tag{S15}$$

where β is a measure for the relative within-species variation of the maximal diameter and c is a normalization constant. We assumed that the maximal diameter for each species can take values $\beta = 20\%$ below the observed maximum. The resulting probability density functions are displayed in Fig. S3.

For technical reasons, we used a discretized version of distribution (S15). To that end, we considered 200 potential maximal DBH values homogeneously distributed in the interval $\left[\min_{s \in \mathcal{S}_i} (1-\beta)\, \bar{d}_s^{\max}, \max_{s \in \mathcal{S}_i} (1-\beta)\, \bar{d}_s^{\max}\right]$.

S2.4.2 Wood density

We computed the wood density of each PFT by taking a weighted average of species-specific wood densities. As weights, we used each species' basal area in the inventory. That is, with weights w_s defined as in equation (S14), we computed the wood

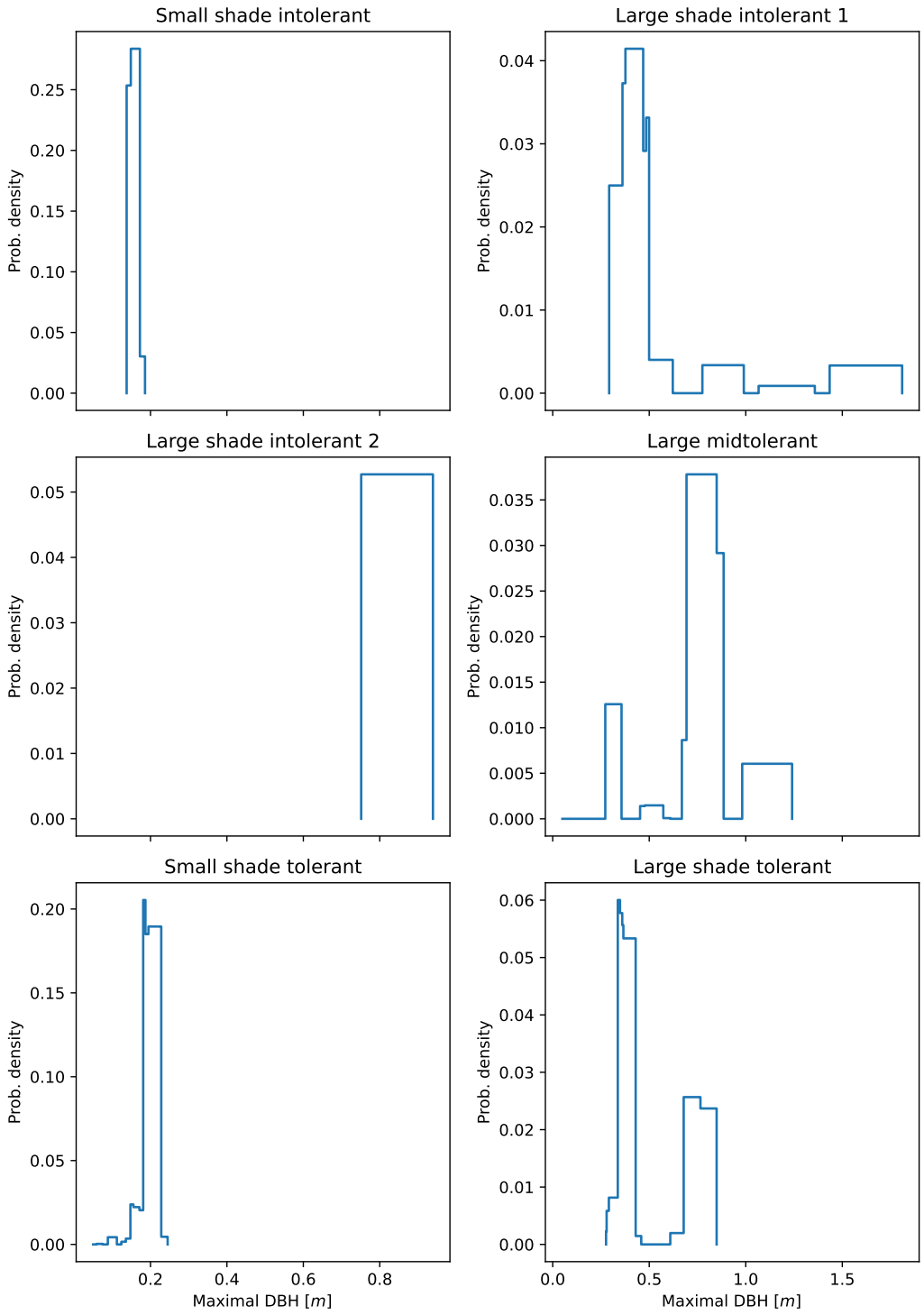

Figure S3. Distribution of the maximal DBH for the six PFTs.

density ρ_i of PFT i via

$$\rho_i = \frac{\sum_{s \in \mathcal{S}_i} \rho_s w_s}{\sum_{s \in \mathcal{S}_i} w_s}, \tag{S16}$$

where ρ_s is the wood density of species s.

S2.4.3 LAI

Both theoretical and empirical studies suggest that a tree's leaf area is roughly proportional to its basal area (West et al., 1999; Xu et al., 2021). However, as it is difficult and costly to determine the leaf area of individual trees, empirical individual-level data on leaf area, leaf number, or LAI are sparse. Xu et al. (2021) estimated leaf numbers as functions of the DBH based on measurements on different branch levels (Liu, 2009) for three species common in our study area. In the absence of more direct measurements, we used a simple approximation based on results by Xu et al. (2021) to parameterize the PFTs to which the species they considered belong and used generic estimates for the other PFTs.

As general ansatz for the relationship between DBH d and LAI L, we used the following function:

$$L(d) = \theta_{\mathrm{LAI},0,i} + \theta_{\mathrm{LAI},1,i} \frac{d^{\theta_{\mathrm{LAI},2,i}}}{A_i(d)}, \tag{S17}$$

where $\theta_{\mathrm{LAI},0,i}$, $\theta_{\mathrm{LAI},1,i}$, $\theta_{\mathrm{LAI},2,i}$ are parameters for PFT i and

$$A_i(d) = \frac{\pi}{4} g_{\text{crown-d}}(d; \theta_{\text{crown-d},i})^2 \tag{S18}$$

is the corresponding crown projection area (see also equation (S9)). The division by the crown projection area $A_i(d)$ transforms leaf area values to LAI values. The intercept parameter is necessary, because trees require a minimal LAI to growth as much as observed in the field. As the crown projection area is roughly proportional to the DBH, the LAI would converge to 0 for small trees if $\theta_{\mathrm{LAI},0,i} = 0$.

We used the exponents $\theta_{\mathrm{LAI},2,i}$ reported by Xu et al. (2021) for *Betula platyphylla*, *Pinus koraiensis* and *Tilia amurensis* for the large shade intolerant 1, large mid-tolerant, and large shade tolerant PFT, respectively. For the other PFTs, we assumed a generic value of 2 (West et al., 1999). We computed the remaining parameters $\theta_{\mathrm{LAI},1,i}$ based on mean LAI values $L_{\mathrm{ref},i}$ reported by Xu et al. (2021). For PFTs with unknown mean LAI, we used a generic value of 3. As it was unclear, to which DBH values the reported mean values corresponded, we set reference DBH values $d_{\mathrm{ref},i}$ dependent on the maximal tree sizes:

	Unit	Small shade intolerant	Large shade intolerant 1	Large shade intolerant 2	Large mid-tolerant	Small shade tolerant	Large shade tolerant
$d_{\mathrm{ref},i}$	m	0.1	0.25	0.25	0.25	0.1	0.25
$L_{\mathrm{ref},i}$	$\frac{\mathrm{m}^2}{\mathrm{m}^2}$	3	11.79*	3	3.717*	3	2.622*
$\theta_{\mathrm{LAI},0,i}$	$\frac{\mathrm{m}^2}{\mathrm{m}^2}$	1	1	1	0.5	0.5	0.5
$\theta_{\mathrm{LAI},1,i}$	$\frac{\mathrm{m}^2}{\mathrm{m}^{\theta_{\mathrm{LAI},2,i}}}$	1581	3373	671.1	654.9	3086	1191
$\theta_{\mathrm{LAI},2,i}$	1	2	2.132*	2	1.847*	2	2.27*

Table S4. Parameter values for the relationship between DBH and LAI. Values marked with an asterisk (*) were taken from Xu et al. (2021).

$0.1\mathrm{m}$ for small PFTs and $0.25\mathrm{m}$ for large PFTs. Setting $L(d_{\mathrm{ref},i}) = L_{\mathrm{ref},i}$, we obtained $\theta_{\mathrm{LAI},1,i}$ with a simple manipulation of equation (S17). The resulting parameter values are displayed in Table S4. The resulting curves are visible in Fig. S2d.

S2.4.4 Light extinction and transmission

To compute the light climate in the forest, parameters for the light extinction and light transmission of leaves are needed. We assumed that these coefficients are independent of the PFTs. For the light extinction coefficients we assumed a value of 0.5 and for the light transmission coefficients a value of 0.1.

S2.4.5 Mean stem biomass proportion

In FORMIND, the biomass of a tree is computed by scaling the stem biomass by an expansion factor, which reflects that some biomass is allocated in branches and leaves. This expansion factor may depend on the tree size and PFT. In our parameterization, we computed the factor based on a submodel described in section S2.7.5 below. However, to parameterize this submodel, we needed information about the mean stem biomass proportions.

We determined the mean proportions of above-ground biomass in the tree crown (i.e., branches and leaves) by comparing independent biomass estimates (Piponiot et al., 2022) for the Changbaishan forest plot with the biomass estimates obtained via the allometric relationships estimated in the sections above. As the estimates by Piponiot et al. (2022) correspond to the entire forest only, we reimplemented their approach, which is based on the allometric biomass equations presented in Table 5 in Chojnacky et al. (2014). We mapped the species found in the inventory data to the taxa found in the table and used the corresponding biomass equations to estimate the species' respective total biomasses in the study area. For species for which we could not find a matching biomass equation, we used the equation corresponding to Aceraceae with specific gravity below 0.5.

	Small shade intolerant	Large shade intolerant 1	Large shade intolerant 2	Large mid-tolerant	Small shade tolerant	Large shade tolerant
Mean stem biomass prop.	0.8	0.5	0.6	0.7	0.7	0.75

Table S5. Estimated mean stem biomass proportion for the different PFTs.

	Unit	Small shade intolerant	Large shade intolerant 1	Large shade intolerant 2	Large mid-tolerant	Small shade tolerant	Large shade tolerant
$n_{\text{seeds},i}$	$\frac{1}{\text{ha}\cdot\text{yr}}$	1.297	9.997	1.28	4.346	2.603	3.409
$\theta_{\text{est},0}$	1	0.0714	0.202	0.0807	0.0091	0.0405	$3.36{\cdot}10^{-4}$

Table S6. Parameters for seed influx and establishment.

We then adjusted the mean stem biomass proportions until our biomass estimates matched the ones obtained via the equations by Chojnacky et al. (2014). The resulting stem biomass proportions are displayed in Table S5.

S2.5 Seed production and seed mortality

We assume that there is a constant external seed influx to the forest. This assumption holds approximately if the considered forest is part of a larger forest area and seed availability does not depend on local species abundances. The seeds are distributed evenly among the patches. Seeds that do not establish to small trees accumulate in a "seed bank" and may establish in later years. However, seeds in the seed bank are subject to a mortality of 50% per year.

We determined the number $n_{\text{seeds},i}$ of incoming seeds of PFT i by fitting the model to forest inventory data (see section S2.11 for details). The resulting values are displayed in Table S6.

S2.6 Ingrowth

Seeds establish to small trees dependent on the light available at the forest's ground and the length of the productive season. The fraction $\phi_{\text{seed},i}$ of seeds of PFT i that establish is computed using a Hill function:

$$\phi_{\text{seed},i}(\phi_{\text{light},j}) = \frac{\phi_{\text{light}}^{\theta_{\text{est},1}}}{\phi_{\text{light}}^{\theta_{\text{est},1}} + \theta_{\text{est},0,i}^{\theta_{\text{est},1}}}, \tag{S19}$$

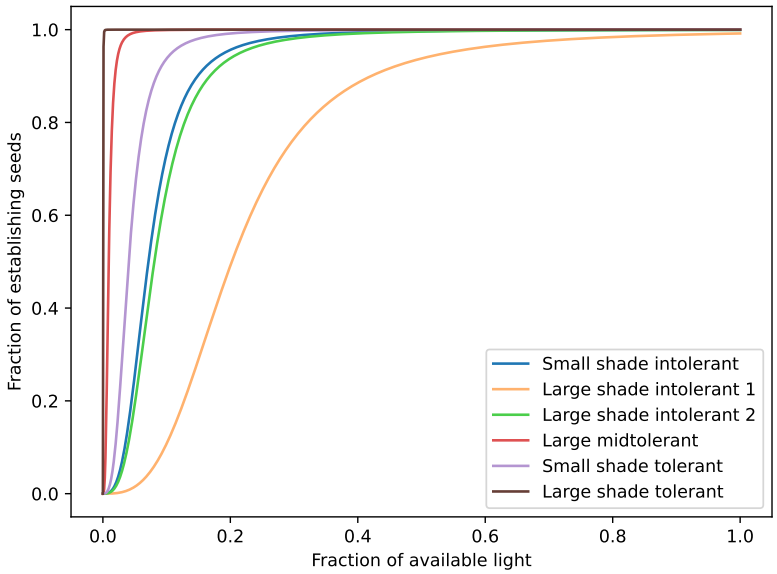

Figure S4. Ingrowth functions for the six PFTs. The fraction of seeds in the seedbank that establish depends on the fraction of irradiation reaching the bottom of the forest as compared to the incoming irradiation.

where $\phi_{\text{light},j} \in [0,1]$ is the fraction of the incoming irradiance that reaches the ground in patch j, the parameter $\theta_{\text{est},0,i} \in [0,1]$ is the irradiance at which half of the seeds of PFT i germinate, and $\theta_{\text{est},1}$ is a parameter controlling how steep the transition from unfavourable to favourable germination conditions is. We estimated the parameters $\theta_{\text{est},0,i}$ and $\theta_{\text{est},1}$ by fitting the model to forest inventory data (section S2.11). The resulting values for $\theta_{\text{est},0,i}$ are displayed in Table S6; the threshold sharpness was not fitted PFT-specifically and assumed a value of $\theta_{\text{est},1} = 3$. The resulting curves are shown in Fig. S4.

The number $n_{\text{seedling},i,j}$ of newly establishing trees of PFT i in patch j is computed by rounding the product of the number $n_{\text{seedbank},i,j}$ of seeds in the corresponding seed bank and the number of establishing seeds $\phi_{\text{seed},i}(\phi_{\text{light},j})$:

$$n_{\text{seedling},i,j} := \lfloor n_{\text{seedbank},i,j}\phi_{\text{seed},i}(\phi_{\text{light},j}) + 0.5 \rfloor \tag{S20}$$

All newly established trees have an initial DBH of 0.05m irrespective of the PFT.

S2.7 Growth

In FORMIND, the growth of a tree is modelled using multiple interacting submodels, which we calibrated partly jointly and partly independently from one another (see Fig. S5 for an overview). The key idea of our approach was to focus on trees growing under the best possible conditions found on site. Focusing on optimal conditions reduces the complexity while at the

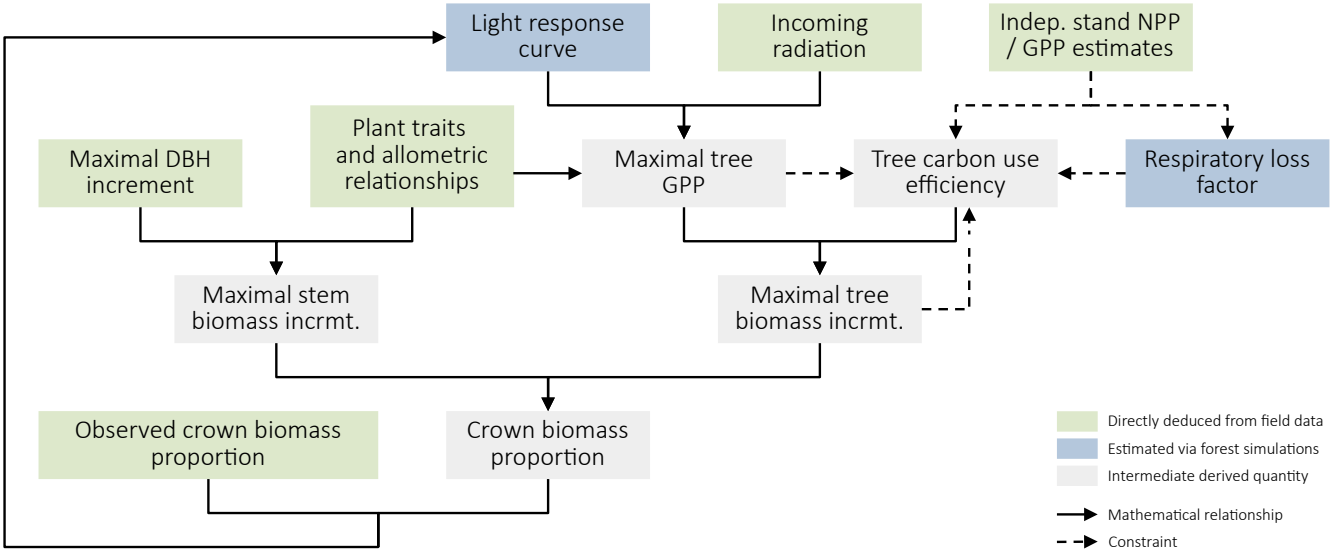

Figure S5. Overview of the model components and intermediate results used to fit the submodels for the growth of individual trees. Solid arrows depict direct mathematical relationships, whereas dashed arrows denote constraints. Submodels and quantities that could be estimated independently from the full model are drawn in green. Submodels with parameters that could only be estimated from the full model are shown in blue. Quantities that were derived from other components are depicted in grey.

same time setting a frame for the possible model behaviour. Below we briefly summarize our approach before providing details in the succeeding sections.

Based on the forest inventory data, we estimated the PFT- and DBH-dependent DBH increment under optimal conditions (section S2.7.1) and used this along with the estimated allometric relationships (section S2.3) and plant traits (section S2.4) to approximate the stem biomass increment under optimal conditions. At the same time, we used our model to estimate the GPP (section S2.7.3) and carbon use efficiency (section S2.7.4) of trees under optimal growth conditions. In a second step, we computed the aboveground wood production, which we could use along with the observed stem biomass increments to deduce the biomass allocated to the crown (section S2.7.5). We compared these values with field estimates, in turn, to refine the parameters that we used to compute the GPP. Parameters that could not be estimated with this procedure were estimated by fitting the full forest model to the forest inventory data (section S2.11).

S2.7.1 DBH increment under optimal conditions

We estimated the DBH increment under optimal conditions based on the DBH increments observed in consecutive forest inventory data. We modelled the DBH increment as observed in the inventory data via a simple stochastic model and used this as a baseline to derive the optimal DBH increment.

We assumed that the DBH increment $\Delta d_{i_k}(d_k)$ of a tree k with PFT i_k and DBH d_k follows a Gamma distribution. Specifically,

$$\Delta d_i(d) \sim \mathrm{Gamma}\left(\frac{\mu_{\Delta\mathrm{DBH},i}(d)}{\theta_{\Delta\mathrm{DBH}}}, \theta_{\Delta\mathrm{DBH}}\right), \tag{S21}$$

where $\mu_{\Delta\mathrm{DBH},i}(d)$ is the DBH-dependent mean DBH increment, and $\theta_{\Delta\mathrm{DBH}}$ is a scale parameter controlling the distributions mean to variance ratio, which we assumed to be independent of the DBH. We assumed that

$$\mu_{\Delta\mathrm{DBH},i}(d) = \theta_{\Delta\mathrm{DBH},i,0} + \theta_{\Delta\mathrm{DBH},i,1} d + \theta_{\Delta\mathrm{DBH},i,2} d^2 + \theta_{\Delta\mathrm{DBH},i,3} d^3 \tag{S22}$$

is a cubic polynomial satisfying the following constraints:

$$\mu_{\Delta\mathrm{DBH},i}(d_i^{\max}) = 0, \tag{S23}$$

$$\mu_{\Delta\mathrm{DBH},i}(0) \geq 0, \tag{S24}$$

$$\mu'_{\Delta\mathrm{DBH},i}(0) \geq 0, \tag{S25}$$

$$\mu'_{\Delta\mathrm{DBH},i}(d_i^{\max}) \leq 0, \tag{S26}$$

where $d_i^{\max}$ is the maximal DBH a tree of PFT i can assume. Constraint (S23) reflects that trees with DBH $d_i^{\max}$ cannot grow even under optimal conditions. Together with constraints (S24)-(S26), it follows that $\mu'_{\Delta\mathrm{DBH},i}$ is always non-negative and at most unimodal in the interval $[0, d_i^{\max}]$. Note that constraint (S23) implies that one of the parameters $\theta_{\Delta\mathrm{DBH},i,0}, \ldots, \theta_{\Delta\mathrm{DBH},i,3}$ can be expressed in terms of the other ones, reducing the degree of freedom when fitting the model.

We estimated the parameters by maximizing the likelihood given data from consecutive forest inventories, conducted in intervals of five years. For each tree k that appeared in two consecutive inventories, we determined the observed DBH difference

$$\Delta d_k^{\mathrm{obs}} = d_{k,t_2} - d_{k,t_1}, \tag{S27}$$

where $d_{k,t}$ is the observed DBH of tree k in year t and $\Delta t = t_2 - t_1 = 5\,\mathrm{yr}$. As empirical data may always be prone to error, we disregarded all data that were more than 5 standard deviations apart from the mean DBH increment, taken over all individuals of the considered PFT. Afterwards, we also excluded all negative values $\Delta d_k^{\mathrm{obs}} < 0$. We estimated the parameters for the optimal

	Unit	Small shade intolerant	Large shade intolerant 1	Large shade intolerant 2	Large mid-tolerant	Small shade tolerant	Large shade tolerant
$\theta_{\Delta\mathrm{DBH}}$	1	$7.607{\cdot}10^{-4}$	$9.939{\cdot}10^{-4}$	$1.361{\cdot}10^{-3}$	$1.110{\cdot}10^{-3}$	$6.554{\cdot}10^{-4}$	$1.171{\cdot}10^{-3}$
$\theta_{\Delta\mathrm{DBH},i,0}$	m	$1.013{\cdot}10^{-3}$	$1.299{\cdot}10^{-3}$	$5.552{\cdot}10^{-4}$	$1.276{\cdot}10^{-3}$	$7.098{\cdot}10^{-4}$	$9.300{\cdot}10^{-4}$
$\theta_{\Delta\mathrm{DBH},i,1}$	1	$3.354{\cdot}10^{-3}$	0	0	0	$7.866e{\cdot}10^{-3}$	0
$\theta_{\Delta\mathrm{DBH},i,2}$	$\frac{1}{\mathrm{m}}$	$1.665{\cdot}10^{-2}$	$9.564{\cdot}10^{-3}$	$1.771{\cdot}10^{-2}$	$9.321{\cdot}10^{-3}$	$-2.317{\cdot}10^{-2}$	$1.324{\cdot}10^{-2}$
$\theta_{\Delta\mathrm{DBH},i,3}$	$\frac{1}{\mathrm{m}^2}$	$-2.084{\cdot}10^{-1}$	$-5.344{\cdot}10^{-3}$	$-1.848{\cdot}10^{-2}$	$-7.820{\cdot}10^{-3}$	$-3.957{\cdot}10^{-2}$	$-1.601{\cdot}10^{-2}$

Table S7. Parameters for the DBH increment distributions.

DBH growth by fitting the distribution (S21) to the values

$$\Delta\bar{d}_k^{\mathrm{obs}} = \frac{\Delta d_k^{\mathrm{obs}}}{\Delta t}. \tag{S28}$$

The resulting parameter estimates are displayed in Table S7. In Fig. S6, we show histograms for the observed DBH increments and the density functions of the corresponding fitted Gamma distributions.

The Gamma distribution can take arbitrarily large values. Our goal, however, was to determine some "maximal" DBH increment. We assumed that the maximal DBH increment is given by some (high) quantile $q_{\Delta\mathrm{DBH}}$ of the fitted DBH increment distribution:

$$\Delta d_{\max,i}(d) = F^{-1}_{\Delta d_i(d)}(q_{\Delta\mathrm{DBH}}), \tag{S29}$$

where $F^{-1}_{\Delta d_i(d)}$ is the inverse cumulative probability density function of $\Delta d_i(d)$. That is, the DBH under optimal conditions is the value chosen so that a fraction of $q_{\Delta\mathrm{DBH}}$ of the DBH increments of similar trees are expected to be lower. Whereas we estimated the distribution of the DBH increments from forest inventory data, we fitted the parameter $q_{\Delta\mathrm{DBH}}$ along with other parameters based on a dynamic forest simulation (see section S2.11). We obtained a value of $q_{\Delta\mathrm{DBH}} = 0.991$. The resulting curves for the DBH-dependent optimal DBH increment are displayed in Fig. S7.

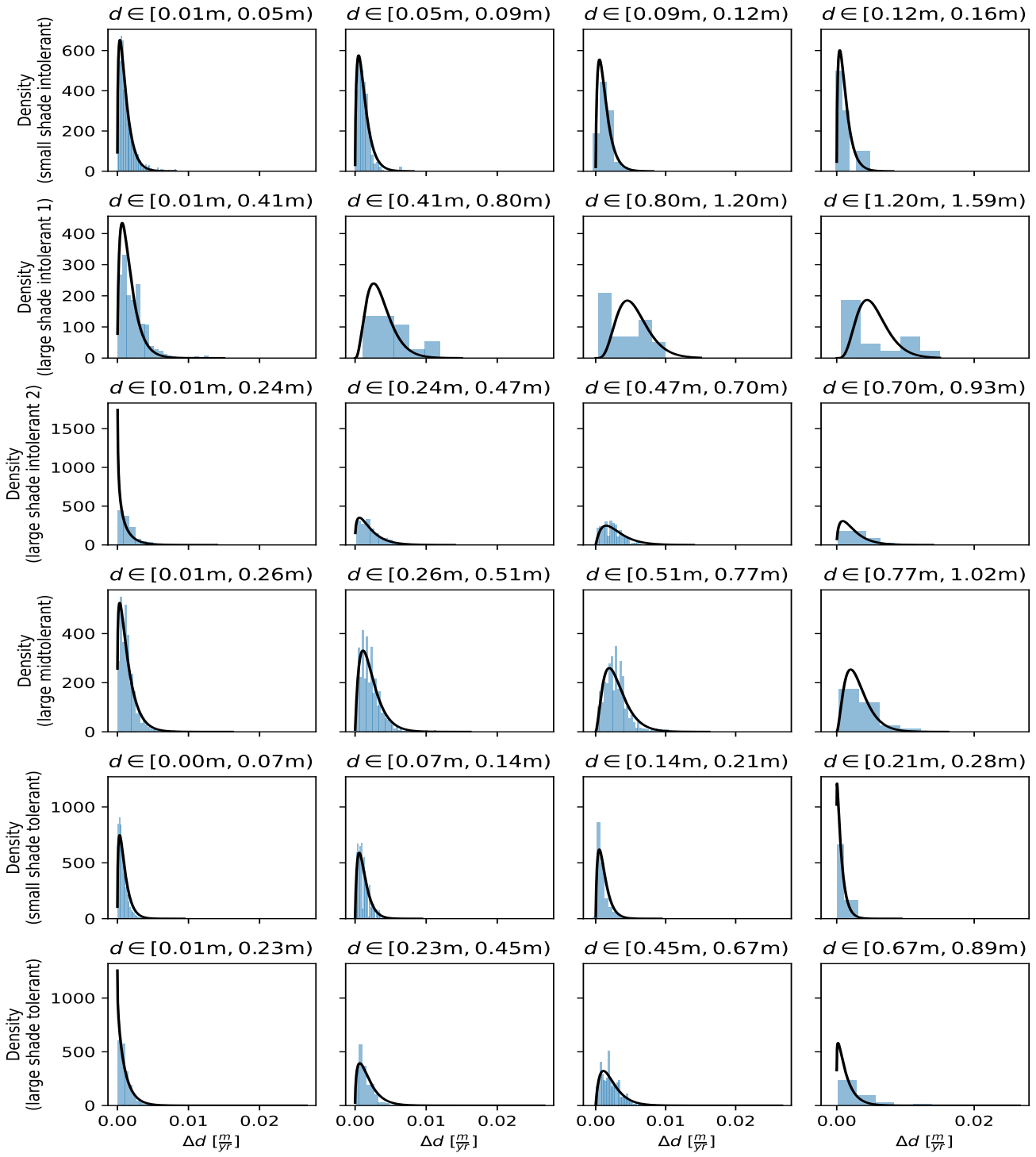

Figure S6. Histogram of observed DBH increments (blue histograms) and fitted DBH increment used in the model (black lines) for the six PFTs and plant sizes. Each panel corresponds to a PFT (indicated in the row description) and a size class (range of considered DBH indicated in the panel heading). The observed DBH increments are averages over five year periods. The plotted probability densities correspond to the DBHs in the centre of the respective considered DBH interval.

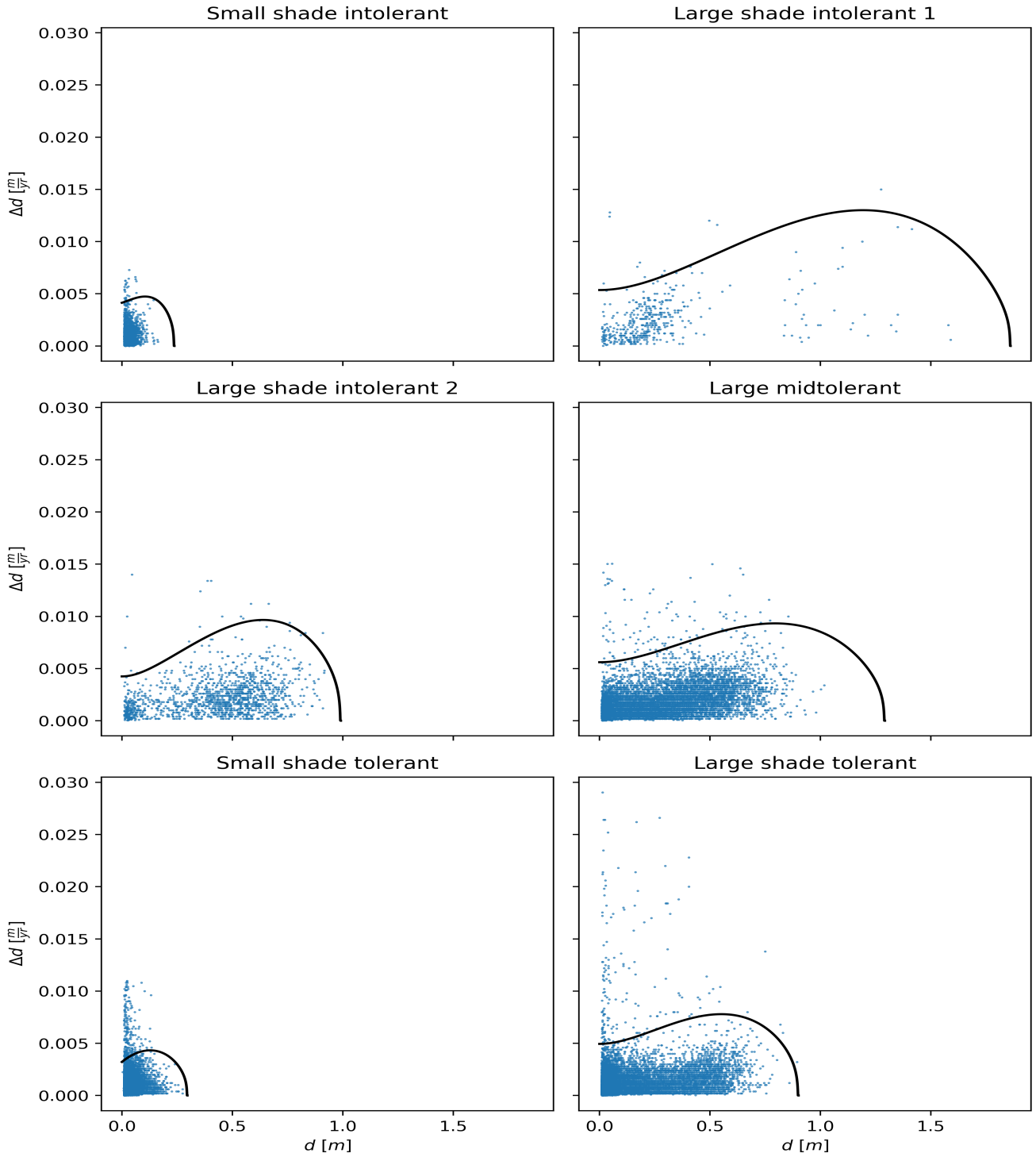

Figure S7. Observed yearly DBH increments (blue dots) and maximal DBH increment used in the model (black lines) for the six PFTs.

S2.7.2 Reference conditions

We assumed that the estimated optimal DBH increments (section S2.7.1) were obtained under the best possible conditions found at the Changbaishan site. To link these observed DBH increments to the modelled GPP, we needed to model these reference conditions explicitly. We assumed that the optimal growth conditions correspond to the best light conditions observed in the forest inventory. For large trees, this is equivalent to being unshaded by other trees. However, there may be no unshaded small trees in the inventory for some PFT, requiring us to adjust the reference light conditions accordingly. This issue was not considered in previous paramterizations of FORMIND. This may have led to underestimated growth of small trees.

Here, we made an ad-hoc correction to account for the range of light conditions found for trees in the inventory. We initialized FORMIND with the forest inventory data, computed the incoming light for all trees (Fig. S8), and determined a simple piecewise linear function that yields for each DBH the maximal fraction of incoming radiation observed for trees with this DBH

$$\phi_{\text{light}}(d) = \min(\theta_{\text{light},0} + \theta_{\text{light},1} d, 1)$$

where $\theta_{\text{light},0}$ is the most favourable fraction of irradiance received by small plants and $\theta_{\text{light},1}$ is the initial slope of the reference light fraction. We fitted this curve via visual inspection, observing (1) the approximate maximal irradiance received by small trees and (2) the DBH at which some trees received the full irradiance. We obtained the values $\theta_{\text{light},0} = 0.5$ and $\theta_{\text{light},1} = 1.5625\text{m}^{-1}$. The resulting relation is displayed in Fig. S8.

S2.7.3 Light response curve

In FORMIND, a tree's GPP is determined based on the light response curve mapping the incoming radiation I_{leaf} of a leaf of PFT i to its photosynthetic rate P_{leaf}

$$P_{\text{leaf},i}(I_{\text{leaf}}) = \frac{\theta_{\text{production},i,0} I_{\text{leaf}}}{\theta_{\text{production},i,1} + I_{\text{leaf}}}, \tag{S30}$$

where $\theta_{\text{production},i,0}$ is the maximal possible photosynthetic rate and $\theta_{\text{production},i,1}$ the irradiation at which half of the maximally possible photosynthetic rate is achieved. We fitted the parameters $\theta_{\text{production},i,1}$ based on model simulations and the forest inventory data (section S2.11). For each given value of $\theta_{\text{production},i,1}$, we computed the corresponding parameter $\theta_{\text{production},i,0}$ by determining how large the production needs to be to let the trees of PFT i attain their observed crown biomass proportions based on our assumptions on the carbon use efficiency (see section S2.7.4) and stem biomass allocation. Details are provided in section S2.7.5.

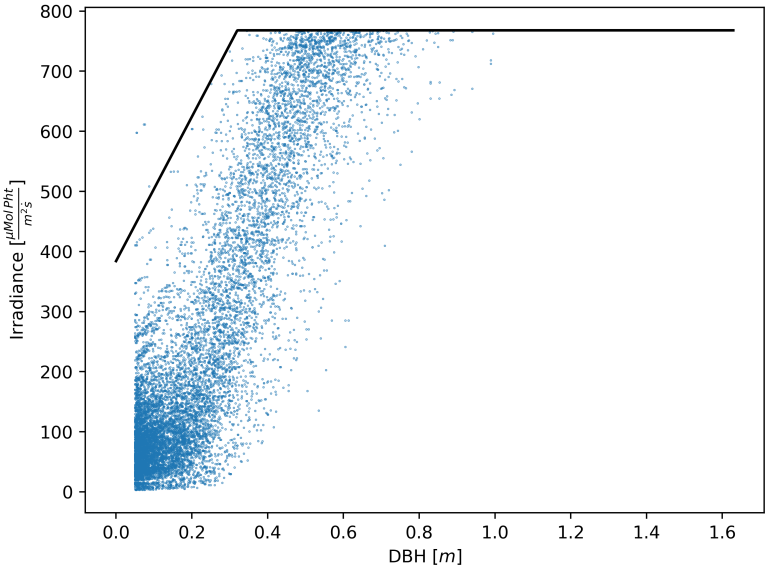

Figure S8. Reference light conditions dependent on the DBH. Each blue dot corresponds to a tree in the inventory and shows its DBH and the irradiance that it received according to the shading model in FORMIND. The black line depicts the irradiance that is used as "optimal" reference in the parameterization. As there are no unshaded small trees, the estimated maximal observed DBH increment (section S2.7.1) does not correspond to unshaded trees. Therefore, the black curve starts at an irradiance 50% below the irradiance received by unshaded trees.

	Unit	Small shade intolerant	Large shade intolerant 1	Large shade intolerant 2	Large mid-tolerant	Small shade tolerant	Large shade tolerant
$\theta_{\text{production},i,0}$	$\frac{\mu\text{Mol}\,\text{CO}_2}{\text{m}^2\cdot\text{s}}$	13.677	4.864	5.274	3.459	3.215	11.553
$\theta_{\text{production},i,1}$	$\frac{\mu\text{Mol photon}}{\text{m}^2\cdot\text{s}}$	500	118.56	100	70.82	274.15	492.73

Table S8. Parameters for the light response curve.

S2.7.4 Carbon use efficiency and respiration

We define the carbon use efficiency (CUE; in formulas C_k) of a tree k as the fraction of its primary production (GPP; in formulas P_k) that is used for net (aboveground) primary production (NPP, in formulas ΔB_k):

$$C_k = \frac{\Delta B_k}{P_k}. \tag{S31}$$

The NPP, in turn, can be written as the difference of GPP and respiration:

$$\Delta B_k = P_k - R_k. \tag{S32}$$

We considered two types of respiratory losses: the maintenance respiration $R_{\mathrm{maint},i}(d)$, dependent on the tree size but independent of the GPP, and other losses and limitations $R_{\mathrm{loss},k}$, proportional to the NPP but otherwise independent of the tree size:

$$R_k = R_{\mathrm{maint},i}(d_k) + R_{\mathrm{loss},k} = R_{\mathrm{maint},k} + \frac{\gamma_{i_k}}{1-\gamma_{i_k}}\Delta B_k = R_{\mathrm{maint},k} + \gamma_{i_k}\left(P_k - R_{\mathrm{maint},k}\right),$$

where γ_{i_k} is a PFT-dependent loss factor, modelling how much of the production not assigned to maintenance can be used for production. It follows

$$\begin{aligned} C_k &= \frac{P_k - R_{\mathrm{maint},k} - \gamma_{i_k}\left(P_k - R_{\mathrm{maint},k}\right)}{P_k} \\ &= (1-\gamma_{i_k})\left(1 - \frac{R_{\mathrm{maint},k}}{P_k}\right) \end{aligned} \tag{S33}$$

Note that the maintenance respiration represents the tree's minimal respiratory needs and thus cannot be reduced even if the tree is under stress. Hence, if the maintenance respiration is large compared to the other losses, already a moderate reduction of the GPP (e.g. due to shading) can entail that a tree cannot satisfy its respiratory needs and stops growing or dies.

As no data on the optimal CUE on single-tree level were available to us, we created a phenomenological model for the *optimal* CUE (below: OCUE) based on a number of observations:

1. The OCUE decreases as trees grow in size.
2. The OCUE must be sufficiently large that trees can reach the estimated optimal biomass increment.
3. The CUE must suffice that most trees observed in the inventory can satisfy their minimal respiratory needs.
4. The order of magnitude of the OCUE must be chosen so that the values of GPP and NPP match field measurements on the stand level approximately.
5. The OCUE is subject to additional limitations and carbon losses independent of the maintenance respiration. Hence the OCUE cannot exceed $1 - \gamma_i$.

As baseline for the OCUE model, we used the following formula:

$$C_{\mathrm{base},i}(d) = \theta_{\mathrm{OCUE},0,i} - \theta_{\mathrm{OCUE},1,i} d^{\theta_{\mathrm{OCUE},2,i}}, \tag{S34}$$

where i is the PFT, d is the DBH, and $\theta_{\mathrm{OCUE},0,i}$, $\theta_{\mathrm{OCUE},1,i}$, and $\theta_{\mathrm{OCUE},2,i}$ are parameters. However, to guarantee that constraint 2 is satisfied, we also computed the minimal required CUE so that the trees can grow as much as observed under optimal conditions. Let

$$\Delta B^{\mathrm{opt}}_{\mathrm{stem},i}(d) = \rho_i \left(V_{\mathrm{stem},i}(d + \Delta d_{\mathrm{max},i}(d)) - V_{\mathrm{stem},i}(d) \right) \tag{S35}$$

be the stem biomass increment under optimal conditions, where d is the current DBH, ρ_i is the wood density, $V_{\mathrm{stem},i}$ the stem volume, and $\Delta d_{\mathrm{max},i}$ the DBH increment under optimal conditions. We assumed that, under optimal conditions, at least a factor $\kappa_{\min} = 0.1$ of the NPP is allocated to crown growth. Hence, the NPP under optimal conditions must be at least $\frac{1}{1-\kappa} \Delta B \Delta B^{\mathrm{opt}}_{\mathrm{stem},i}(d)$. Consequently, we adjusted the OCUE correspondingly:

$$C_{\mathrm{opt},i}(d) = \max\left(C_{\mathrm{base},i}(d), \frac{1}{1-\kappa_{\min}} \Delta B^{\mathrm{opt}}_{\mathrm{stem},i}(d) \right). \tag{S36}$$

We assumed that the OCUE is monotonously decreasing as trees grow. With constraint 5, we obtain that $\theta_{\mathrm{OCUE},0,i} \leq \gamma_i$. At the same time, constraint 3 requires that $R_{\mathrm{maint},i}(d)$ is small for small trees, as small shaded trees observed in the inventory could not survive otherwise. Hence, we set

$$\theta_{\mathrm{OCUE},0,i} = \gamma_i - 0.01. \tag{S37}$$

Similarly, applying the shading module of FORMIND to the inventory data, we observed that the OCUE must decrease slowly for small trees (Fig. S9), which in turn requires a sufficiently large exponent $\theta_{\mathrm{OCUE},2,i}$. We therefore set $\theta_{\mathrm{OCUE},2,i} = 3$ for all PFTs i. Lastly, we determined $\theta_{\mathrm{OCUE},1,i}$ so that the largest possible trees of PFT i have an OCUE of 0 at their maximal DBH. That is, if

$$d_{\mathrm{max},i} = \sup\{d;\, f_i^{\max}(d) > 0\} \tag{S38}$$

	Unit	Small shade intolerant	Large shade intolerant 1	Large shade intolerant 2	Large mid-tolerant	Small shade tolerant	Large shade tolerant
γ_i	1	0.15	0.285	0.4	0.4	0.189	0.236

Table S9. Scaling factors relating the NPP to respiratory losses other than the maintenance respiration.

is the maximal DBH a tree of PFT i can attain (cf. equation (S15)), then

$$\theta_{\mathrm{OCUE},1,i} = \theta_{\mathrm{OCUE},0,i} d_{\max,i}^{-\theta_{\mathrm{OCUE},2,i}}. \tag{S39}$$

We estimated the loss factors γ_i by fitting the full model to the inventory data (section S2.11). However, to satisfy constraint 4, we constrained the loss factors γ_i to the interval $[0.6, 1]$ to match the relatively low CUE values observed in the Changbaishan mountain area in independent studies (Piponiot et al., 2022). The resulting parameter estimates are displayed in Table S9

As we assume that the maintenance respiration is independent of a tree's productivity, equation (S33) must in particular hold for trees under optimal growth conditions. Hence, after inserting the fitted OCUE $C_{\mathrm{opt},i}(d)$ and GPP under optimal conditions, equation (S33) can be manipulated to derive the maintenance respiration for a tree of given PFT and DBH.

S2.7.5 Growth allocation

Based on the OCUE and the GPP under optimal conditions, denoted C_i and P_i^{opt}, respectively, we could compute the corresponding NPP $\Delta B_i^{\mathrm{opt}}(d)$ for trees of a given DBH and PFT. Based on the estimated DBH increment under optimal conditions, determined the respective stem biomass increment $\Delta B_{\mathrm{stem},i}^{\mathrm{opt}}(d)$ (see equation (S35)). If $B_i(d)$ is the biomass of a tree of PFT i with DBH d and ζ_i is the corresponding stem biomass proportion, then

$$\begin{aligned}
\Delta B_i^{\mathrm{opt}}(d) &= C_i(d) P_i^{\mathrm{opt}}(d) \\
&= B_i(d + \Delta d_{\max,i}(d)) - B_i(d) \\
&= \frac{B_{\mathrm{stem},i}(d + \Delta d_{\max,i}(d))}{\zeta_i(d + \Delta d_{\max,i}(d))} - \frac{B_{\mathrm{stem},i}(d)}{\zeta_i(d)}
\end{aligned} \tag{S40}$$

$$\iff$$

$$\zeta_i(d + \Delta d_{\max,i}(d)) = \frac{\zeta_i(d) B_{\mathrm{stem},i}(d + \Delta d_{\max,i}(d))}{B_{\mathrm{stem},i}(d) + \zeta_i(d) C_i(d) P_i^{\mathrm{opt}}(d)}. \tag{S41}$$

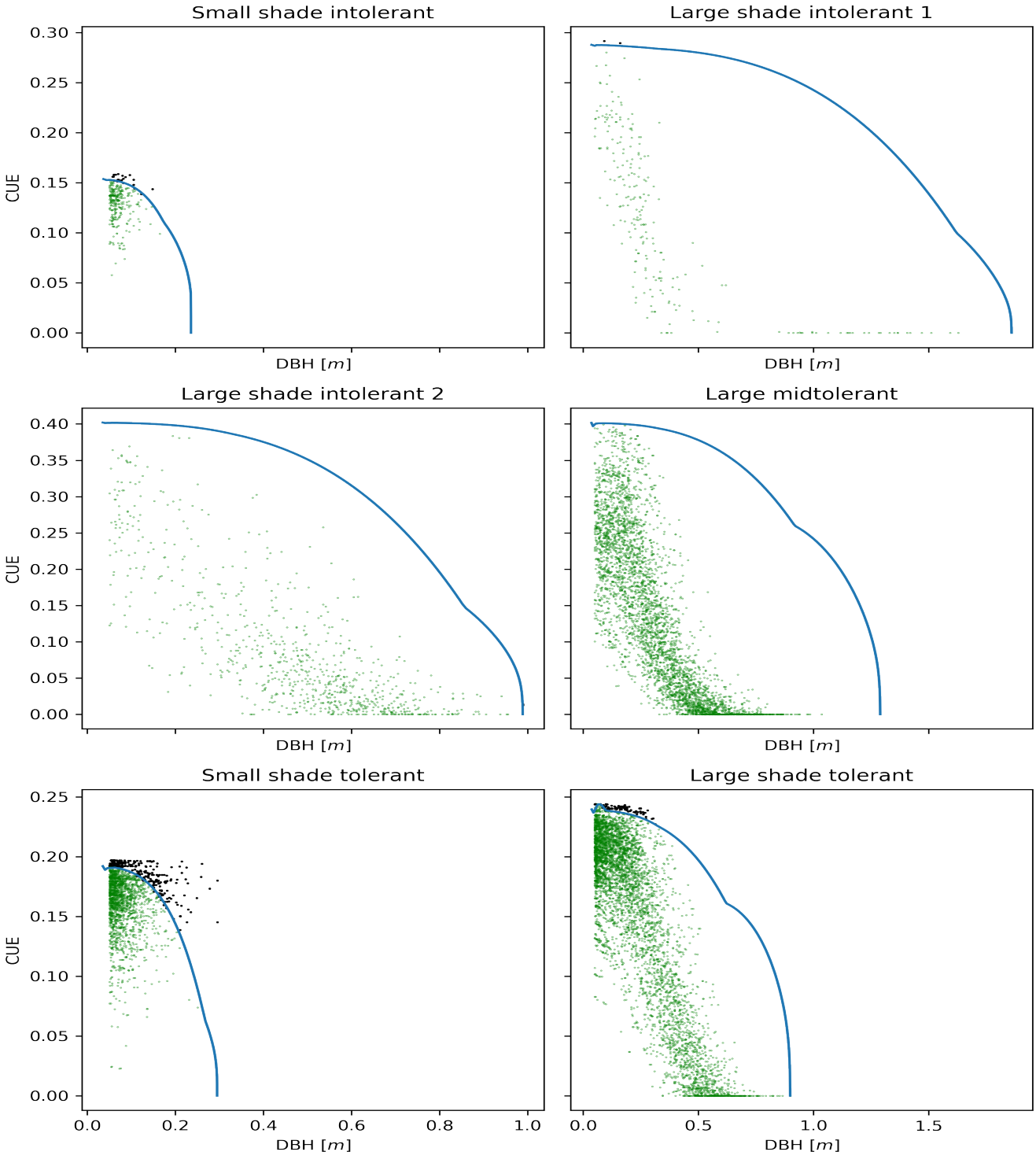

Figure S9. The optimal carbon use efficiency OCUE for the different PFTs. The OCUEs used in the model are depicted as solid blue lines. The points show estimated lower bounds for the required CUEs obtained for trees in the inventory via the shading module of FORMIND. Each point corresponds to a tree; the colour shows whether the tree could satisfy its respiratory needs according to the model (green: yes; black: no). The OCUE curves were chosen so that as many of the points are below the blue curves. The sharp transitions between the curve sections are due to constraint 2 imposing a different shape of the curve for large DBH values (see also equation (S36)).

We used this difference equation to compute the stem biomass proportion for all DBHs and PFTs. We provide details below.

Equation (S41) requires knowledge of the previous stem biomass proportion $\zeta_i(d)$. Hence, we needed initial values for the interval $[d_0, d_0 + \Delta d_{\max,i}(d)]$ with d_0 being the stem diameter of new saplings. These initial values may be chosen arbitrarily. Using a shifted exponential ansatz for the initial condition yielded well-behaved smooth results for ζ_i:

$$\zeta_i(d) = a_{0,i} + a_{1,i}\exp(a_{2,i} \cdot d) \qquad \text{if } d < d_0 + \Delta d_{\max,i}(d_0). \tag{S42}$$

We chose the coefficients a_{0i}, a_{1i}, a_{2i} so that the curve $\zeta_i(d)$ is continuous, approximately differentiable, and starts at a given initial value $\zeta_{0i} = \zeta_i(d_0)$.

To see how the coefficients were determined, first note that in practice, the curve ζ_i is computed numerically and hence evaluated at a discrete set of sampling points only. We chose the sampling points so that they have a constant distance to one another. Intermediate values were obtained via linear interpolation between these points. Now, let $d_{1i} = d_0 + \Delta d_{\max,i}(d_0)$, let $\bar{d}_{1i} > d_{1i}$ be the smallest sampling point larger than d_{1i}, and choose $\bar{d}_{0i}$ so that $\bar{d}_{1i} = \bar{d}_{0i} + \Delta d_{\max,i}\big(\bar{d}_{0i}\big)$. Furthermore, define (evaluating equation (S41) at d_{0i} and $\bar{d}_{0i}$)

$$\zeta_{1i} = \frac{\zeta_{0i} B_{\text{stem},i}(d_1)}{B_{\text{stem},i}(d_0) + \zeta_{0i} C_i(d) P_i^{\text{opt}}(d_0)}, \tag{S43}$$

$$\bar{\zeta}_{1i} = \frac{\zeta_{0i} B_{\text{stem},i}\big(\bar{d}_1\big)}{B_{\text{stem},i}\big(\bar{d}_{0i}\big) + \zeta_{0i} C_i(d) P_i^{\text{opt}}\big(\bar{d}_{0i}\big)}. \tag{S44}$$

Now we imposed the following conditions

$$\zeta_i(d_0) = a_{0i} + a_{1i}\exp(a_{2i} \cdot d_0) = \zeta_{0i}, \tag{S45}$$

$$\zeta_i(d_{1i}) = a_{0i} + a_{1i}\exp(a_{2i} \cdot d_{1i}) = \zeta_{1i}, \tag{S46}$$

$$\zeta_i\big(\bar{d}_{1i}\big) = a_{0i} + a_{1i}\exp\big(a_{2i} \cdot \bar{d}_{1i}\big) = \bar{\zeta}_{1i} \tag{S47}$$

and obtained

$$a_{1i} = \frac{\zeta_{1i} - \zeta_{0i}}{\exp(a_{2i} \cdot d_{1i}) - \exp(a_{2i} \cdot d_0)} \tag{S48}$$

$$a_{0i} = \zeta_{0i} - a_{1i}\exp(a_{2i} \cdot d_0). \tag{S49}$$

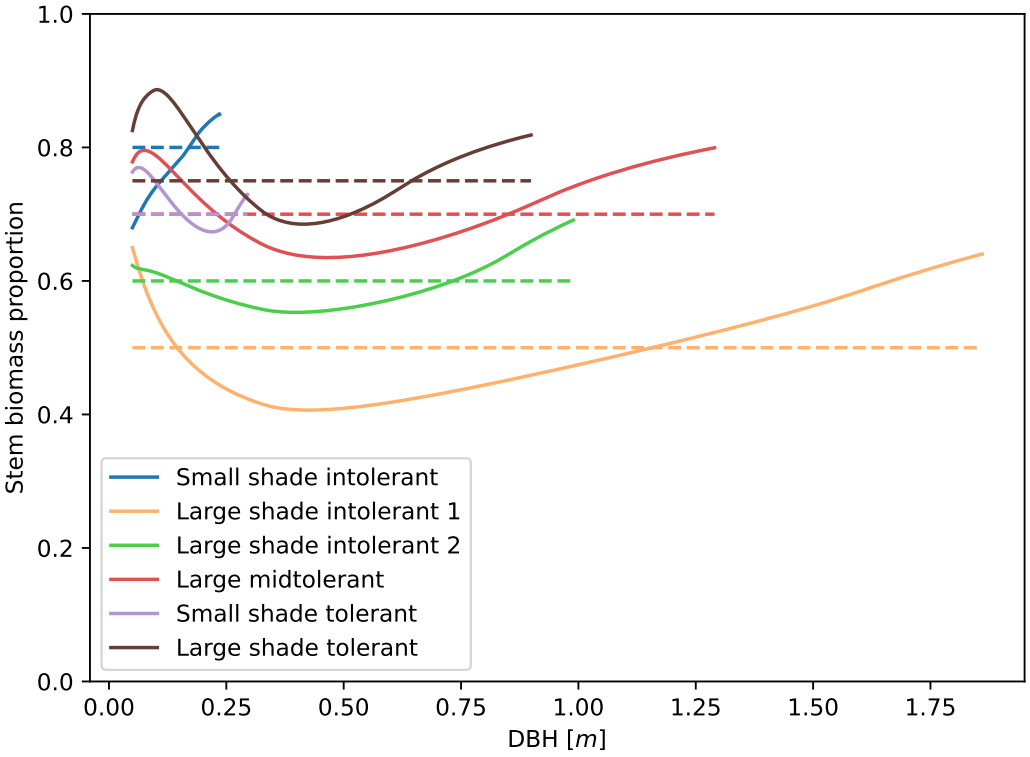

Figure S10. Stem biomass proportions of the six PFTs. The solid lines depict the stem biomass proportions used in the model (obtained via the approach described in section S2.7.5). The dashed lines show the independently estimated mean values (see section S2.4.5).

We computed the remaining unknown coefficient a_{2i} via a binary search on equation (S47) using the values for a_{0i} and a_{1i} from equations (S48)-(S49).

We approximated the mean of the curves $\zeta_i(d)$ by taking the man of the functions values at 50 equidistant points in the intervals $[0.1\text{m}, d_{\text{max},i}]$, respectively. We then conducted a binary search in the maximal possible photosynthetic rate $\theta_{\text{production},i,0}$ (see section S2.7.3) until the approximate mean values matched the mean stem biomass proportions estimated from the field data (section S2.4.5).

S2.7.6 Defoliation

If trees are shaded, it can happen that their maintenance respiration exceeds their GPP. In these cases, we assumed that parts of the crown die until the remaining tree can be maintained. Here, we assumed that for a tree of given DBH, the maintenance respiration is proportional to its biomass. That is, a tree k with insufficient production P_k, maintenance respiration $R_{\text{maint},k}$,

and biomass B_k will reduce its biomass to

$$\tilde{B}_k = B_k \frac{P_k}{R_{\mathrm{maint},k}}, \tag{S50}$$

and its maintenance respiration will be set to P_k. As we assume the biomass is lost in the crown only, the stem biomass proportion is adjusted accordingly to a value $\tilde{\zeta}_k$.

We assumed that the loss in crown biomass also affects the tree's number of leaves and thereby the LAI. We reduced the LAI proportional to the crown completeness

$$\begin{aligned}\eta_k &= \frac{\tilde{B}_{\mathrm{crown},k}}{B_{\mathrm{crown},i_k}(d_k)} \\ &= \frac{\tilde{B}_k - B_{\mathrm{stem},i_k}(d_k)}{B_{i_k}(d_k) - B_{\mathrm{stem},i_k}(d_k)},\end{aligned} \tag{S51}$$

where $\tilde{B}_{\mathrm{crown},k}$ is the reduced crown biomass and $B_{i_k}(d_k)$ the biomass of a tree with complete crown and DBH d_k. As a result, trees with incomplete crowns have reduced GPP and shade other trees less. Trees without any crown biomass ($\eta_k = 0$) cannot recover and die.

We assumed that if the light conditions for a tree with incomplete crown improve, the new biomass is first allocated to "refill" the crown until $\eta_k = 1$. Any remaining new biomass is allocated to the usual tree growth with corresponding DBH increment.

S2.8 Competition

We assumed that trees solely compete for light. In particular, we did not apply crowding mortality. Instead, the forest density is self-regulated via crown defoliation and the resulting tree death. This process has an effect similar to crowding mortality ("full" forests lead to deadly overshadowing of small plants) but a better mechanistic justification. In particular, mortality via light competition incorporates the traits of both the shadowing and the overshadowed trees, since the LAI of larger plants as well as the respiratory demands of smaller plants are parameterized individually for each plant functional type (PFT).

S2.9 Stochastic mortality

We assumed that trees die randomly with probabilities dependent on their PFT and DBH. As model for the mortality, we used a linear combination of exponentials:

$$p_{\mathrm{mort},i}(d) = \theta_{\mathrm{mort},0,\mathrm{i}} + \theta_{\mathrm{mort},1,\mathrm{i}} \exp(\theta_{\mathrm{mort},2,\mathrm{i}} d) + \theta_{\mathrm{mort},3,\mathrm{i}} \exp(\theta_{\mathrm{mort},4,\mathrm{i}} d), \tag{S52}$$

	Unit	Small shade intolerant	Large shade intolerant 1	Large shade intolerant 2	Large mid-tolerant	Small shade tolerant	Large shade tolerant
$\theta_{\mathrm{mort,0,i}}$	1	0	0	0.004	0	0	0
$\theta_{\mathrm{mort,1,i}}$	1	0.0568	0.0345	0.2415	0.0829	0.0106	0.0224
$\theta_{\mathrm{mort,2,i}}$	1	−9.5049	−12.6546	−43.2337	−10.6963	5.6635	−3.0862
$\theta_{\mathrm{mort,3,i}}$	1	0	0.0112	$6.823{\cdot}10^{-5}$	0.002	0	0
$\theta_{\mathrm{mort,4,i}}$	1	0	0.5339	5.0046	1.8684	0	0

Table S10. Parameters for the mortality probabilities.

where $p_{\mathrm{mort},i}(d)$ is the probability that a tree of PFT i and DBH d dies within a year. This model may take a variety of shapes including mortality increasing or decreasing with plant size or a "bathtub" shape, where the mortality is lowest for plants with intermediate sizes.

We estimated the parameters in equation (S52) using data from consecutive forest inventories. We determined which trees died in the intermediate time by comparing which trees that were present in the first inventory were also present in the second inventory. For simplicity, we assumed that the tree DBH does not change significantly during the 5 year period between two censuses and that random mortality is the only death mechanism at play. If d_{k,t_1} is the DBH observed in the inventory in year t_1, the probability that the tree survived until the year t_2 of the second inventory is approximately

$$p^{\mathrm{obs}}_{\mathrm{mort},i_k} = \left(1 - p_{\mathrm{mort},i_k}(d_{k,t_1})\right)^{t_2 - t_1}. \tag{S53}$$

We used this to construct the likelihood for the observed death and survival events. We then estimated the parameters in equation (S52) for the different PFTs. The resulting parameters are displayed in Table S10 and the resulting curves in Fig. S11.

Besides the random mortality, we trees may die due to strong light competition (see section S2.7.6) or by falling large trees. We assumed that trees larger than $0.1\,\mathrm{m}$ may fall with a probability of 0.4 and kill smaller trees. Details of this mechanism are described in Fischer et al. (2016).

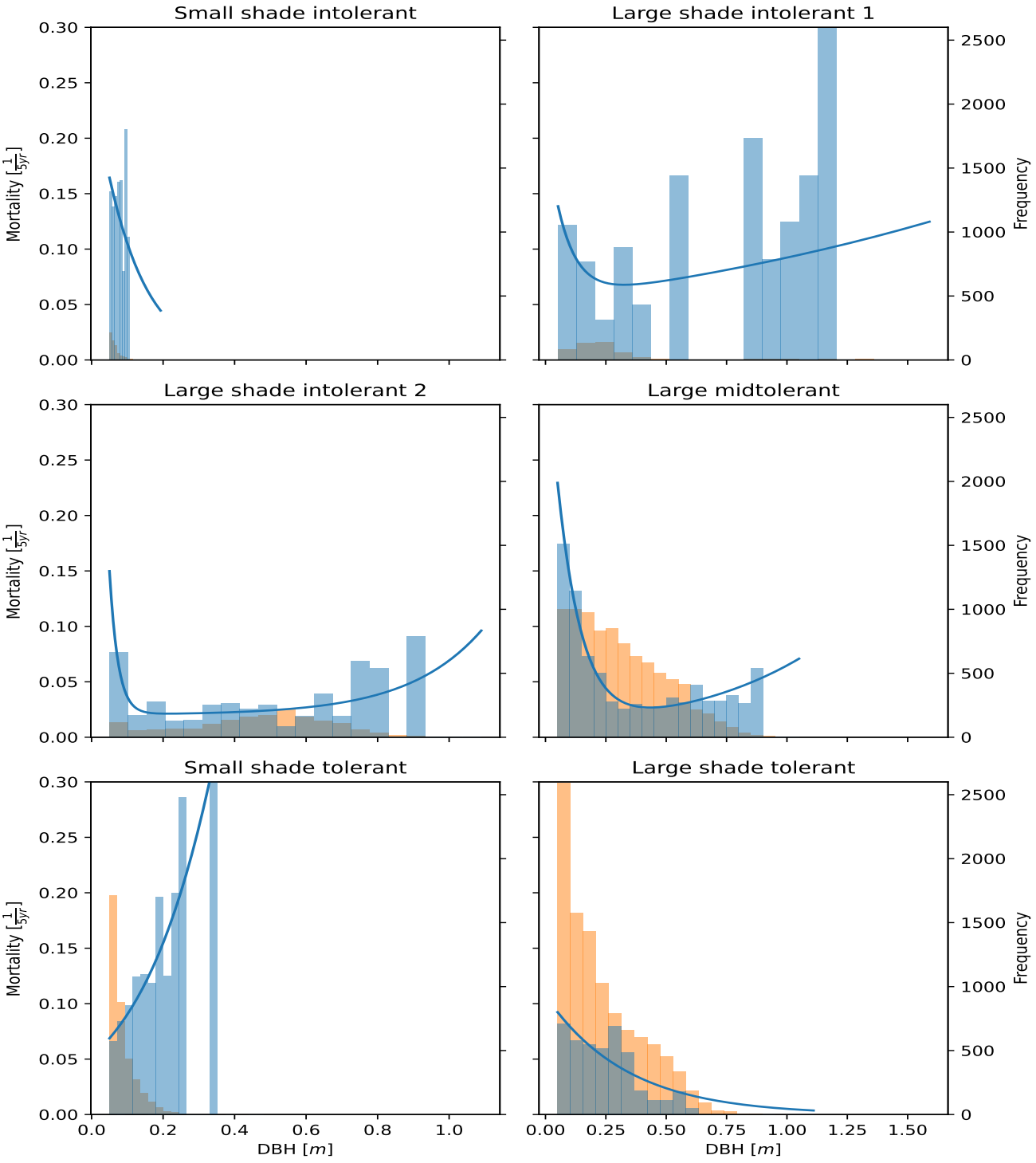

Figure S11. Mortality by PFT (field data and model). The blue curves (primary axis) depict the modelled DBH-dependent probabilities that a tree dies within a year. The blue bars correspond to field estimates of the death probabilities (number of dead trees divided by the total number of trees in the inventory). The orange bars (secondary axis) are a histogram for the tree sizes, indicating where the mortality estimates have the strongest empirical support.

S2.10 Climate

We used a static climate in our simulations. Advanced features such as the soil water module, temperature effects, and daily changes to the climate were not included. Instead, we used averaged values, which we provide below.

Evapotranspiration. For the mean actual evapotranspiration, we used a value of $600\frac{\mathrm{mm}}{\mathrm{yr}}$. This is in line with independent estimates for the Changbaishan region (Sun et al., 2004) and earlier parameterizations of the model for temperate forests (Bohn et al., 2014).

Growing season. We defined the growing season as the months with positive mean temperature. This were the months March until October (Wang et al., 2020).

Irradiance. We computed the mean yearly light intensity ("PAR") above the canopy during daytime in the growing season based on the WFDEI forcing dataset (Weedon et al., 2014). We obtained a value of $768\frac{\mu\mathrm{Mol\,photons}}{\mathrm{m}^2}$.

Day length. We computed the average length of a day in the growing season and obtained a value of $13.39\mathrm{h}$.

S2.11 Fitting procedure

Some parameters were not available from the literature and could not be determined directly from the available data. We estimated these parameters based on dynamical forest simulations and the inventory data (see Fig. S12). After a burn-in period, we generated a sample of forest states via simulations. Then, we used the generated sample to estimate the likelihood for the parameters given the inventory data via kernel density estimation (KDE). We then optimized the parameters by maximizing the likelihood. Below we provide details for each of the steps involved.

S2.11.1 Forest state characterization

We characterized the forest's state by determining the stem count and the biomass in the considered patch for each PFT. That is, the state space was 12-dimensional. The combined information of stem count and biomass yields basic insight into the size distribution of trees, as a large stem count with small biomass indicates a young forest with many small trees, and a small stem count with high biomass indicates an old forest with few large trees. Hence, these summary statistics provide relatively rich information about the overall forest state.

We considered forest states on the $20\mathrm{m} \times 20\mathrm{m}$ level. For the forest plot in Changbaishan, which has a size of $25\mathrm{ha}$, we therefore obtained a sample of 625 observed forest states.

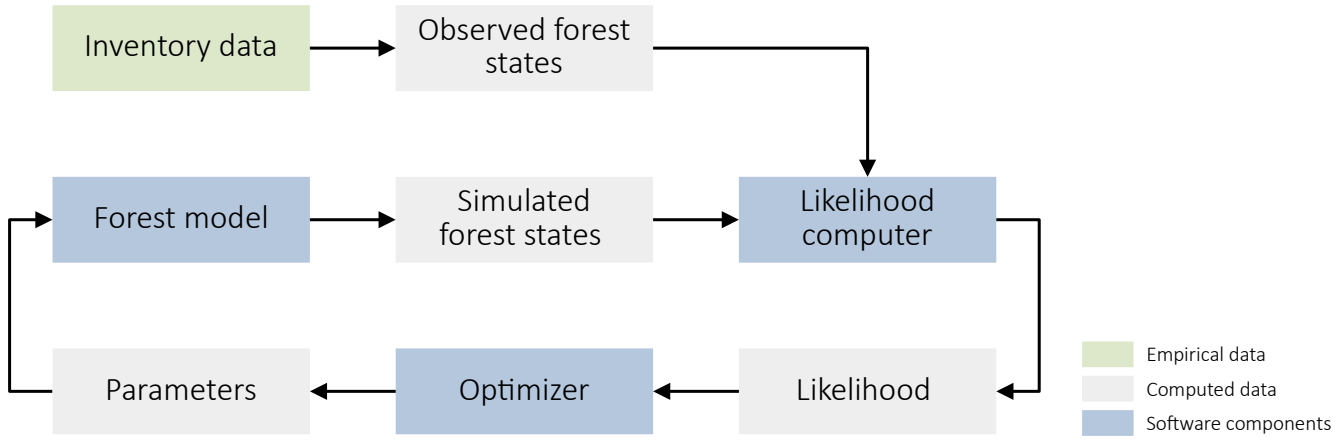

Figure S12. Overview of the model fitting procedure.

S2.11.2 Sample generation

To generate a sample of forest states from the model, we first simulated $1\mathrm{ha}$ of forest until it reached its limiting behaviour ($2000\mathrm{yr}$). Then, we generated a sample of forest states on the $20\mathrm{m} \times 20\mathrm{m}$ scale by sampling the forest 500 times every $5\mathrm{yr}$. Via parallel simulations, we repeated this procedure 67 times. That way we obtained a sample of forest states with $n_{\mathrm{sample}} = 837,500$ entries.

In FORMIND, the interactions between $20\mathrm{m} \times 20\mathrm{m}$ patches are small (only via tree falling, which is a rare event). Furthermore, taking samples over a relatively long period of $2500\mathrm{yr}$ reduces the temporal correlations between the generated samples. Therefore, and because we also conducted 67 mutually independent simulations, the generated sample is approximately identically independently distributed.

S2.11.3 Likelihood estimation

The distribution of the forest states according to the forest model is not known in closed form and can only be studied via simulations. Therefore, we estimated the probability density, and based on this the likelihood for the parameters given the data, from the model-generated sample of forest states. To this end, we used kernel density estimation (KDE; Wand and Jones, 1995). In KDE, the probability density f of an element y of the state space is estimated as the mean of kernel functions centred at the elements x_i of the generated sample:

$$f\big(y; x_1, \ldots, x_{n_{\mathrm{sample}}}\big) \approx \hat{f}\big(y; x_1, \ldots, x_{n_{\mathrm{sample}}}\big) \quad = \quad \frac{1}{n_{\mathrm{sample}}} \sum_{i=1}^{n_{\mathrm{sample}}} \prod_{j=1}^{n_{\mathrm{dim}}} K(y_j, x_{ij}; h_j), \tag{S54}$$

where $\hat{f}$ is the estimated probability density, n_{sample} is the number of generated sample points, n_{dim} is the dimension of the state space, K is the kernel function, and h_j is a bandwidth parameter defining the (marginal) scale on which two points are considered approximately similar. Due to its computational simplicity on the log-scale, we used a Gaussian Kernel. However, since stem counts and biomasses are constrained to the non-negative range, we applied reflecting boundary conditions:

$$K_j(y_j, x_{ij}; h_j) = \begin{cases} \frac{1}{w_j}\left(\exp\left(-\frac{(x_{ij}-y_j)^2}{2h_j^2}\right) + \exp\left(-\frac{(x_{ij}+y_j)^2}{2h_j^2}\right)\right) & \text{if } y_j \geq 0 \\ 0 & \text{else} \end{cases} \tag{S55}$$

with $w_j = \sqrt{2\pi}h_j$. For the stem counts, we furthermore needed to normalized the kernel to correctly account for the discrete nature of the data:

$$K_j(y_j, x_{ij}; h_j) = \begin{cases} \frac{1}{w_j}\left(\exp\left(-\frac{(x_{ij}-y_j)^2}{2h_j^2}\right) + \exp\left(-\frac{(x_{ij}+y_j+1)^2}{2h_j^2}\right)\right) & \text{if } y_j \geq 0 \\ 0 & \text{else} \end{cases} \tag{S56}$$

with

$$w_j \quad = \quad 2\sum_{k=0}^{\infty} \exp\left(-\frac{k^2}{2h_j^2}\right) - 1.$$

The bandwidths we used are displayed in Table S11.

KDE provides unbiased estimate of probability densities. For likelihood optimization, however, we need the log-likelihood, because working with the original likelihood would require us to handle extremely small numbers, which is numerically infeasible. As taking the logarithm of a random variable changes its distribution and, in particular, expected value, we applied a bias correction. First, note that for a Gaussian kernel, the KDE's expected value μ_{KDE} and variance σ^2_{KDE} can be approximated as follows (Wand and Jones, 1995):

$$\mu_{\text{KDE}} \approx f(y) \tag{S57}$$

$$\sigma^2_{\text{KDE}} \approx \frac{\mu_{\text{KDE}}}{2\sqrt{\pi}nh}. \tag{S58}$$

We desired to find a bias correction function g so that

$$\mathbb{E}\left(g\left(\hat{f}(y)\right)\right) = \ln \mu_{\text{KDE}}. \tag{S59}$$

State variable	Unit		Small shade intolerant	Large shade intolerant 1	Large shade intolerant 2	Large mid-tolerant	Small shade tolerant	Large shade tolerant
Stem count	$\frac{1}{400\mathrm{m}^2}$	Mean	0.48	0.376	1.278	6.381	3.17	8.229
		Range	$[0,7]$	$[0,8]$	$[0,7]$	$[0,21]$	$[0,17]$	$[0,25]$
		Bandw.	0.4	0.4	0.6	1	0.6	2
Biomass	$\frac{t\,\mathrm{ODM}}{400\mathrm{m}^2}$	Mean	0.06	0.457	2.633	4.617	0.062	3.047
		Range	$[0,0.1]$	$[0,10.945]$	$[0,17.346]$	$[0,13.133]$	$[0,0.607]$	$[0,10.909]$
		Bandw.	0.005	0.05	0.1	0.5	0.02	0.5

Table S11. Ranges and KDE bandwidths for the considered state variables. The bandwidth is the scale in the state space on which a data point in the simulated sample is considered "similar" to a point in the inventory dataset.

Applying a Taylor expansion about μ_{KDE}, we find

$$\begin{aligned}\mathbb{E}\Big(g\Big(\hat{f}(y)\Big)\Big) &\approx g(\mu_{\mathrm{KDE}}) + \frac{1}{2}g''(\mu_{\mathrm{KDE}})\underbrace{\mathbb{E}\Big(\Big(\hat{f}(y)-\mu_{\mathrm{KDE}}\Big)^2\Big)}_{\sigma^2_{\mathrm{KDE}}} \\ &= g(\mu_{\mathrm{KDE}}) + \frac{\sigma^2_{\mathrm{KDE}}}{2}g''(\mu) \\ &\stackrel{!}{=} \ln \mu_{\mathrm{KDE}}. \end{aligned} \tag{S60}$$

We solved differential equation (S60) to obtain the bias correction function, into which we inserted the original results (S54) from the KDE. To avoid numerical issues, we performed all these steps on the log scale.

To fit the model, we considered a 12-dimensional state space. As a result, the products of the kernel functions in equation (S54) can become very small and very sensitive to stochastic differences between simulation runs. We therefore estimated the probability density for each PFT independently and multiplied the results to obtain the joint density. This is equivalent to assuming that the states of different PFTs are mutually independent. Though this assumption is inaccurate in general, using the resulting composite likelihood still yields consistent parameter estimates (Varin, 2008).

S2.11.4 Parameter optimization

A challenge when maximizing the kernel density estimate of the likelihood is that this estimate is stochastic. This requires the applied optimizers to be robust against stochastic fluctuations. We applied the algorithm PY-BOBYQA (Cartis et al., 2019)

Parameter	Unit		Small shade intolerant	Large shade intolerant 1	Large shade intolerant 2	Large mid-tolerant	Small shade tolerant	Large shade tolerant
$n_{\text{seeds},i}$	$\frac{1}{\text{ha}\cdot\text{yr}}$	Range	$[0.001, 50]$	$[0.001, 50]$	$[0.001, 50]$	$[0.001, 50]$	$[0.001, 50]$	$[0.001, 50]$
		Guess	2	2	2	2	2	2
$\theta_{\text{est},0}$	1	Range	$[0.01, 0.4]$	$[0.01, 0.4]$	$[0.01, 0.4]$	$[0.001, 0.4]$	$[0.0001, 0.3]$	$[0.0001, 0.3]$
		Guess	0.15	0.15	0.15	0.05	0.01	0.01
$\theta_{\text{production},i,1}$	$\frac{\mu\text{Mol phot.}}{\text{m}^2\cdot\text{s}}$	Range	$[100, 500]$	$[100, 500]$	$[100, 500]$	$[50, 500]$	$[20, 300]$	$[20, 500]$
		Guess	300	300	300	150	100	100
γ_i	1	Range	$[0.15, 0.4]$	$[0.15, 0.4]$	$[0.15, 0.4]$	$[0.15, 0.4]$	$[0.15, 0.4]$	$[0.15, 0.4]$
		Guess	0.3	0.3	0.3	0.3	0.3	0.3
$q_{\Delta\text{DBH}}$	1	Range	$[0.2, 0.9999]$					
		Guess	0.99					
$\theta_{\text{est},1}$	1	Range	$[3, 20]$					
		Guess	5					

Table S12. Parameter bounds and initial guesses used for parameter optimization.

on a preconditioned version of the log-likelihood function. To reduce numerical issues, we optimized all parameters on the log-scale except for $q_{\Delta\text{DBH}}$, for which we applied an inverse logit transform to constrain it to the open interval $(0, 1)$. Then, we evaluated the log-likelihood function 10 times at the initial parameter guess (Table S12) to estimate its standard deviation. Based on this, we conducted for each parameter individually a rough binary search to find the scale of change on which the log-likelihood function changed by at least 2 standard deviations but not more than 10 standard deviations. We scaled the parameters accordingly for an efficient search. This scaling process is called preconditioning.

We constrained the parameters to ecologically reasonable ranges, respectively. The bounds we applied are displayed in Table S12. To avoid getting stuck due to stochastic deviations, we terminated the search algorithm after 200 likelihood evaluations and restarted the search until a total of 8 runs was completed. To minimize the risk of converging to a local minimum, we furthermore applied basin-hopping (Wales and Doye, 1997) as implemented in Scipy. This algorithm performs repeated local optimizations with randomly perturbed initial conditions. For the perturbation, we applied a step size of 4 on the preconditioned parameter scale. We ran the algorithm for 5 iterations. After finishing this optimization process, we repeated it, using the result as initial value and baseline for preconditioning for the repetition.

S3 DBH entropy

S3.1 Derivation of the DBH entropy

We used the basal-area-weighted DBH entropy as a proxy for the prevalence of large trees in a forest patch. The entropy of the weighted DBH distribution is defined as follows:

$$\tilde{S}_{\mathrm{DBH}} = -\sum_{d \in D} p_d \ln(p_d), \tag{S61}$$

where D is the set of distinct DBH values occurring in the forest patch and

$$p_d = \frac{\sum_{k \in \mathcal{I}: d_k = d} d_k^2}{\sum_{k \in \mathcal{I}} d_k^2}. \tag{S62}$$

is the probability to randomly select a tree with DBH d from the forest patch if the probabilities were proportional to the trees' respective basal areas. Here, $\mathcal{I}$ is the set of trees in the inventory and d_k is the DBH of tree k.

Formula (S61) is sensitive to arbitrarily small changes in DBH values, as trees need to have exactly the same DBH values to be considered similar in equation (S62). This is inappropriate, as DBH values come from a continuous domain, and will never be exactly equal in practice. To make the measure more robust, we could consider DBH intervals instead of individual DBH values, as suggested in the main text. However, this approach is sensitive to the choice of interval bounds and can lead to strongly different results for slight changes of DBH values (cf. Wand and Jones, 1995). We therefore used kernel density estimation to obtain a continuous distribution of tree sizes from the inventory. Then, we considered the entropy of the resulting distribution:

$$S_{\mathrm{DBH}} = -\int_0^\infty f_{\mathrm{d}}(\delta) \ln f_{\mathrm{d}}(\delta) \mathrm{d}\delta, \tag{S63}$$

where

$$f_{\mathrm{d}}(\delta) = \sum_{d \in D} w_d K(d, \delta; h) \tag{S64}$$

with weights

$$w_d = \frac{d^\eta}{\sum_{d \in D} d^\eta} \tag{S65}$$

is the smoothed DBH distribution in the forest patch,

$$K(d, \delta; h) = \begin{cases} \frac{3}{4h}\left(1 - \left(\frac{d-\delta}{h}\right)^2\right) & \text{if } |d - \delta| \leq h \\ 0 & \text{else} \end{cases}$$

is the Epanechnikov kernel, η is the exponent parameter and h is a bandwidth parameter, defining the scale on which two trees are regarded similar.

S3.2 DBH entropy parameterization

The DBH entropy depends on the exponent parameter η and the bandwidth parameter h. In line with our requirements for a proxy for the prevalence of mature trees, we chose $\eta = 2$ to obtain weights by basal area and $h = 1\,\mathrm{cm}$ for a sufficiently fine-grained resolution to distinguish tree sizes well. To validate this choice of parameters and compare it to parameters used in other studies, we assessed the relationship between GPP, NPP, and NEE and the DBH entropy computed with different parameter values: $\eta = 0$ (no weighting), $\eta = 2$ (weighting by basal area), $\eta = 3$ (higher-order weighting, potentially similar to biomass) with $h = 1\,\mathrm{cm}$, respectively, and $\eta = 0$ and $\eta = 2$ with $h = 10\,\mathrm{cm}$. We used the same methods as for the analysis of the other diversity measures.

The results are displayed in Figs. S13 and S14 for the $0.04\,\mathrm{ha}$ and the $1\,\mathrm{ha}$ scale, respectively. It is visible that weighting the entropy by the basal area strengthened the relationhip with the GPP and NEE on the fine scale; for the $1\,\mathrm{ha}$ scale the relationship to the NEE became slightly weaker compared to the unweighted version of the entropy. However, weighting with a higher exponent ($\eta = 3$) worsened the results. Using a larger bandwidth, i.e., counting more trees as similar, worsened the connection between entropy and NPP and NEE. This is notable, as many studies using the DBH entropy as a measure for structural diversity consider the $1\,\mathrm{ha}$ scale (or larger), use a large bandwidth (e.g. $10\,\mathrm{cm}$; Silva Pedro et al., 2017) and do not weight the trees by basal area (e.g. Dănescu et al., 2016; Silva Pedro et al., 2017; Park et al., 2019).

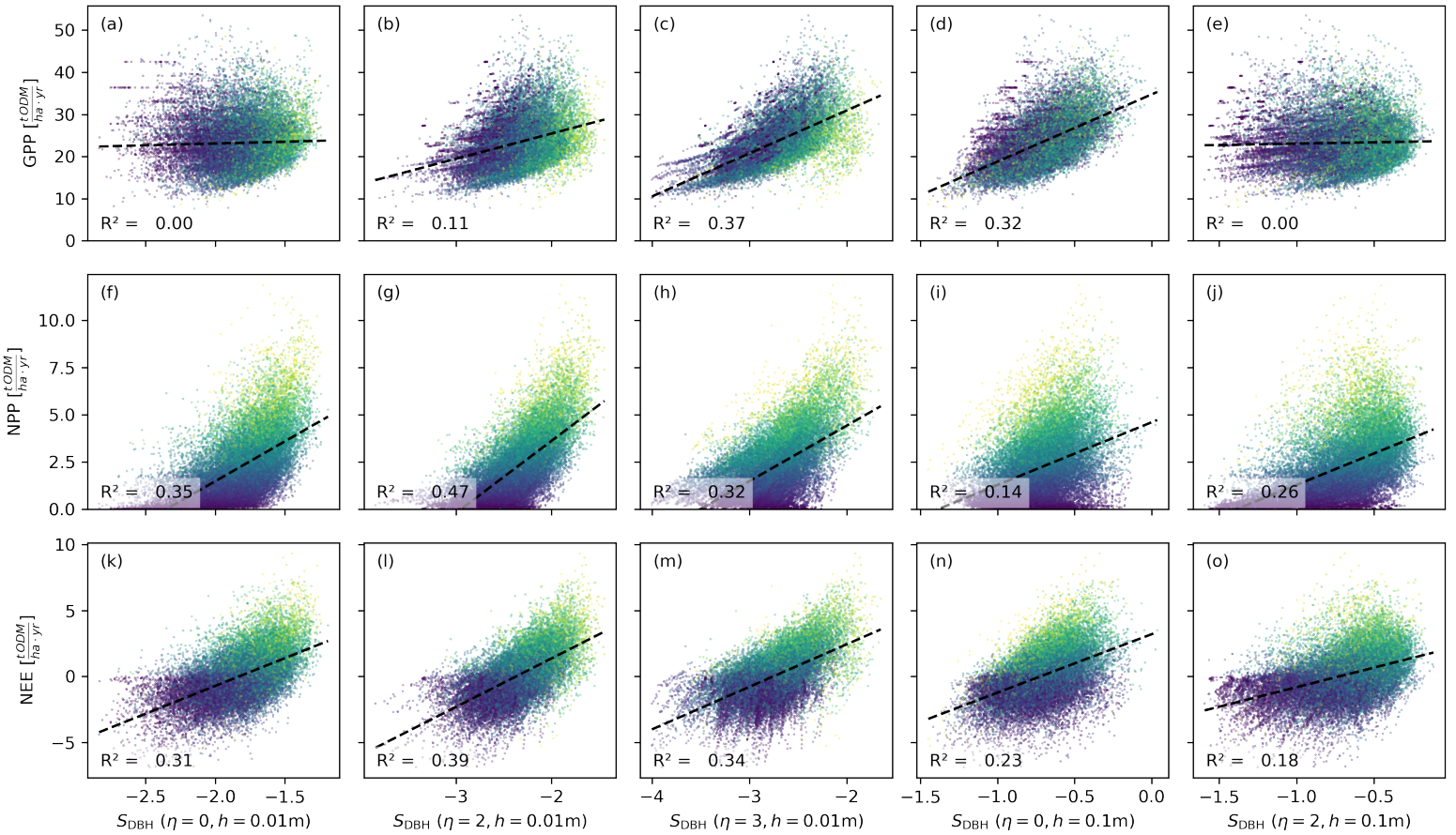

Figure S13. Productivity measures (GPP, NPP, and NEE) dependent on different parameters of the DBH entropy S_{DBH}. Each dot corresponds to a $0.04\,\mathrm{ha}$ forest patch. The colour indicates the basal area proportion of mature trees (blue: only mature trees; yellow: no mature trees). The relationship between entropy and NPP or NEE is strongest if the entropy is computed with weights based on the basal area ($\eta = 2$) and a small bandwidth $h = 1\,\mathrm{cm}$, at which trees are considered similar.

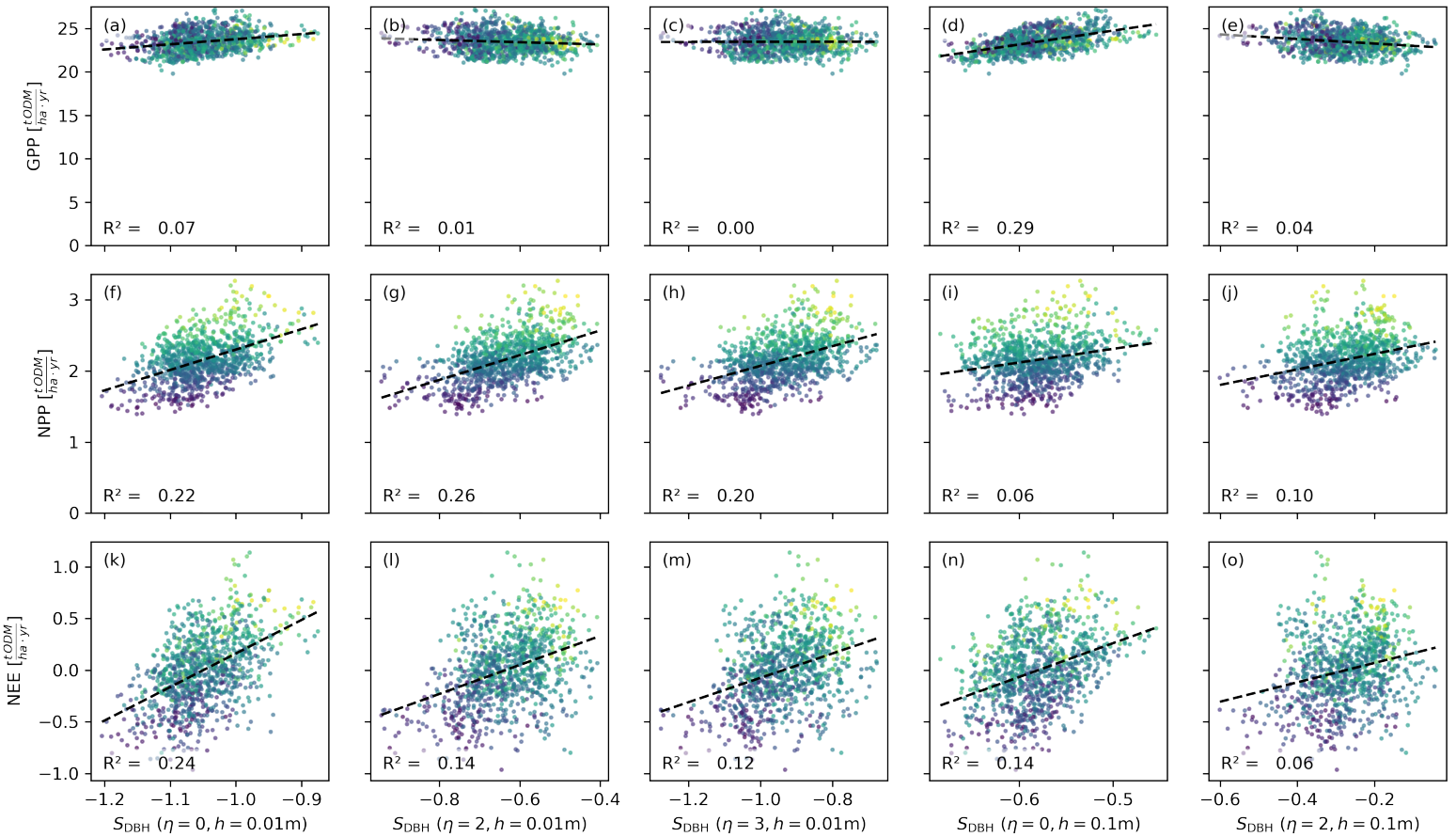

Figure S14. Productivity measures (GPP, NPP, and NEE) dependent on different parameters of the DBH entropy S_{DBH}. Each dot corresponds to a $1\,\mathrm{ha}$ forest patch. The colour indicates the basal area proportion of mature trees (blue: only mature trees; yellow: no mature trees). The relationship between entropy and NPP is strongest if the entropy is computed with weights based on the basal area ($\eta = 2$) and a small bandwidth $h = 1\,\mathrm{cm}$, at which trees are considered similar. For the NEE, the relationship is stronger if the unweighted DBH distribution is used ($\eta = 0$).

S4 Model validation

To verify that our optimization procedure reliably yields good fitting results, we repeated the fitting procedure three times. We obtained estimated log-likelihood values of -4850.32, -4853.39, and -4866.18, respectively. Though already log-likelihood differences of 2 are significant in likelihood ratio tests and for confidence intervals, we consider the fitting procedure successful, because the stochastic optimization problem we needed to solve to fit the model is computationally difficult.

The parameter estimates we obtained in the three optimization runs are displayed in Table S13. For most parameters, the results remained in similar orders of magnitude, suggesting that the parameters are estimable despite remaining uncertainties resulting from the difficulty of the optimization problem. Only the parameter $\theta_{\mathrm{est},1}$ which controls the sharpness of the light threshold for seedling establishment took on vastly different values. This suggests that this parameter may not be estimable and may be set to a predefined value without affecting the goodness of fit significantly.

To validate that our model fits the biomass and stem count distributions from the forest inventory well, we compared a model-generated sample of these values to the sample from the inventory data that was also used in the fitting procedure. We simulated $1\,\mathrm{ha}$ of forest for a burn-in period of $2000\,\mathrm{yr}$ and sampled 25 patches ($0.04\,\mathrm{ha}$) of the simulated forest 1000 times in time intervals of $5\,\mathrm{yr}$. We repeated this procedure 8 times, obtaining a sample with $200,000$ entries, corresponding to a forest of $8000\,\mathrm{ha}$.

Based on the simulated data and the field data, we created one-dimensional histograms of the biomass and stem count for each PFT. Then we plotted these histograms to study how well they overlap. The results are displayed in Figures S15 and S16, respectively. The distributions match reasonably well, indicating a good model fit in light of the model's complexity and the large number of model features fitted simultaneously.

To also evaluate the model's ability to reproduce the joint distributions of biomass and stem count for the six PFTs, we created corresponding two-dimensional histograms, displayed in Fig. S17. The distributions from the model generally matched the patterns observed in the field data. However, the field data often covered a broader range of values than observed in the model simulation. This indicates that some sources of variation are still missing in the model.

In addition to comparing the simulation results with forest inventory data, we also computed stand-level forest characteristics (biomass, NPP, GPP, and LAI), which we then compared to estimates from independent studies (see main text). We considered a forest area of the same size ($25\,\mathrm{ha}$) as the area where the inventory was conducted. We simulated this forest for a burn-in period of $1,000\,\mathrm{yr}$. Then, we determined the forest characteristics of interest in each year for a simulation period of $3,000\,\mathrm{yr}$, yielding a quasi-independent sample with $3,000$ entries. We then determined the sample mean and standard deviation of each of the considered characteristics and used the resulting values for model validation.

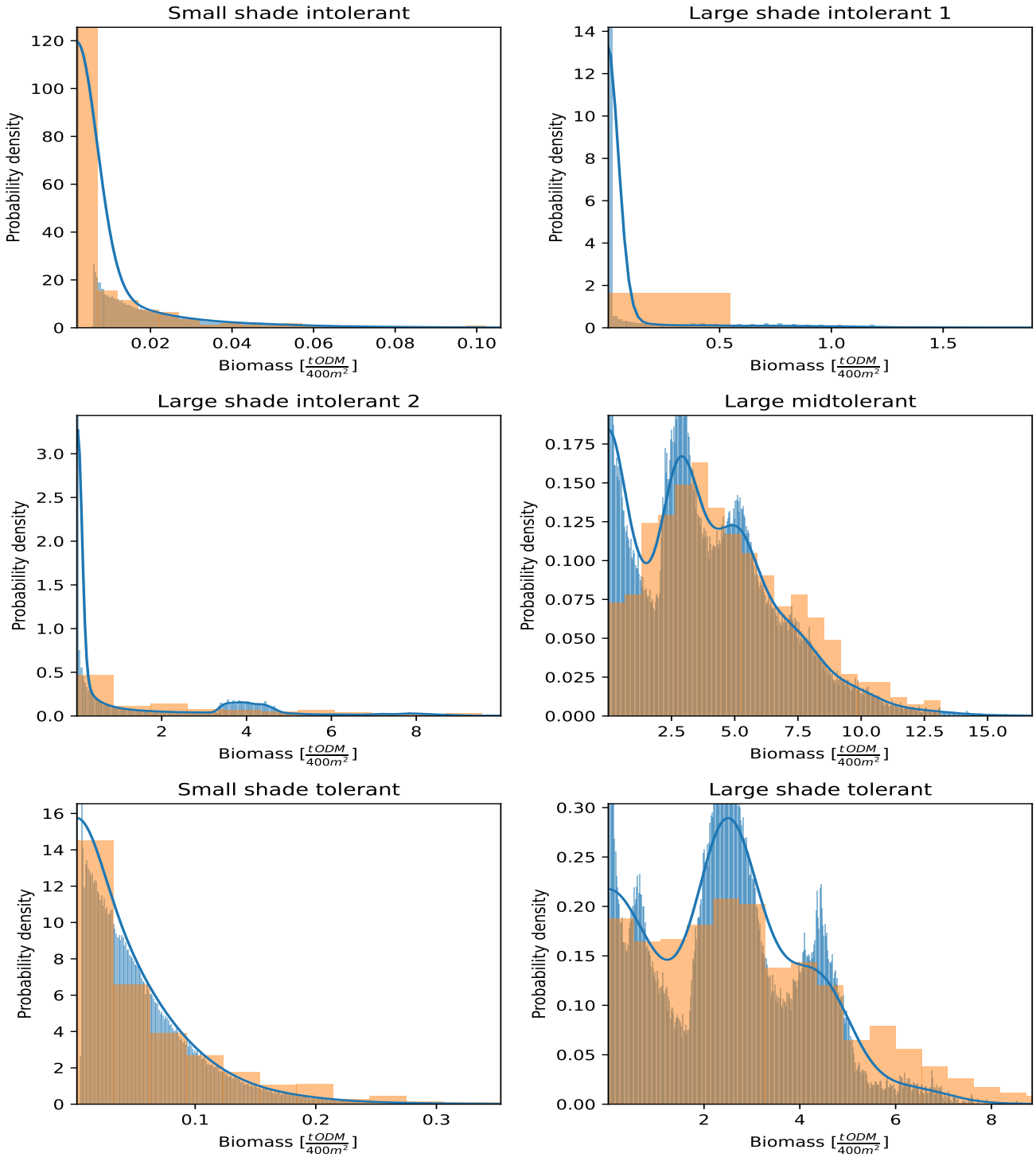

Figure S15. Comparison of the simulated biomass distribution with field data. The figure displays the marginal biomass distribution by PFT on the $0.04\,\mathrm{ha}$ scale. The orange bars form histograms of the biomass estimates generated based on the field data from Changbaishan. The blue bars form histograms of the biomass distributions generated from the model. The blue curves depict the kernel-smoothed density of the distribution used to estimate the likelihood. The distributions obtained from the model generally match the corresponding distributions of the field data well.

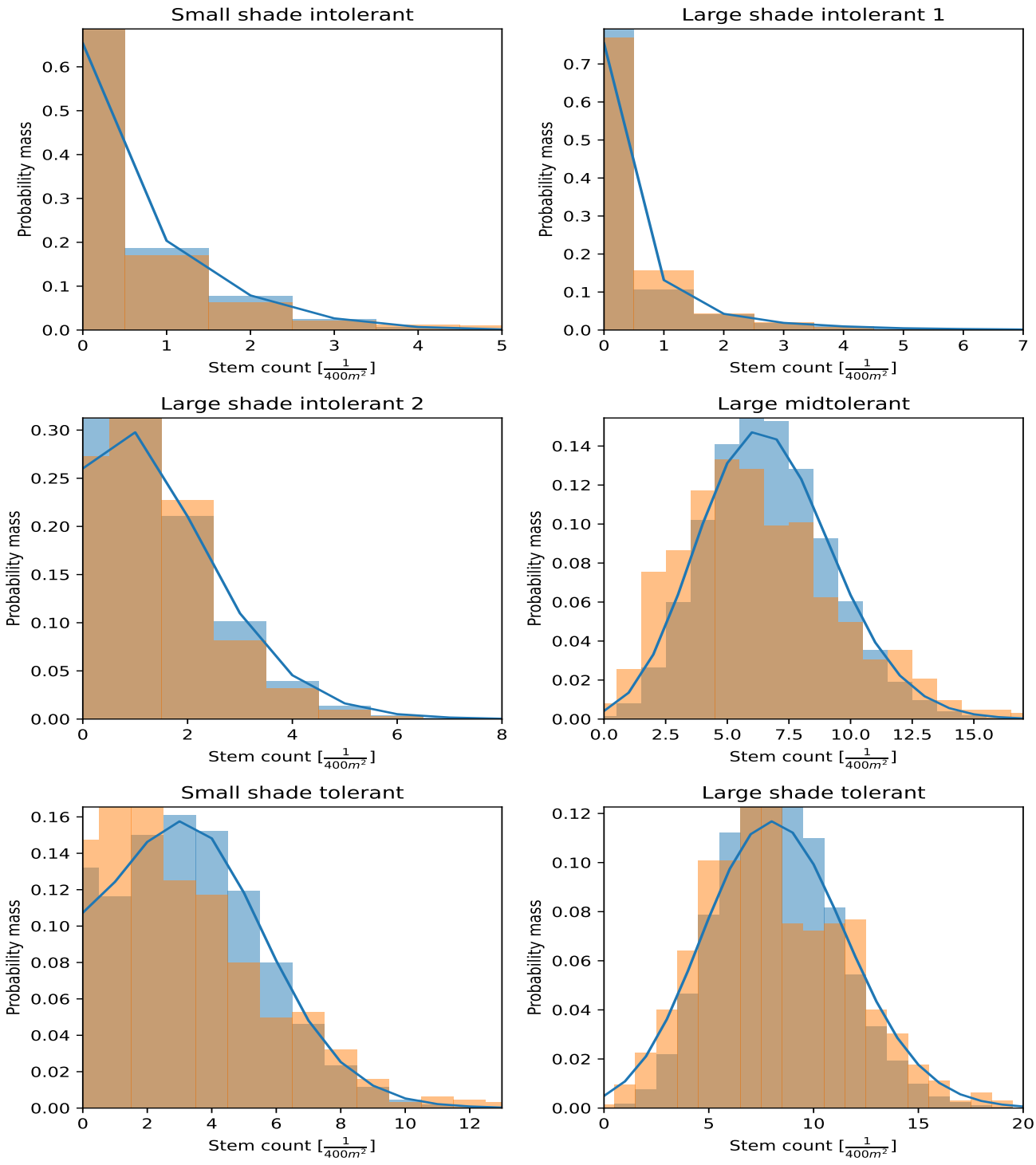

Figure S16. Comparison of the simulated stem count distribution with field data. The figure displays the marginal stem count distribution by PFT on the $0.04\,\mathrm{ha}$ scale. The orange bars form histograms of the stem count estimates generated based on the field data from Changbaishan. The blue bars form histograms of the stem count distributions generated from the model. The blue curves depict the kernel-smoothed density of the distribution used to estimate the likelihood. The distributions obtained from the model generally match the corresponding distributions of the field data well.

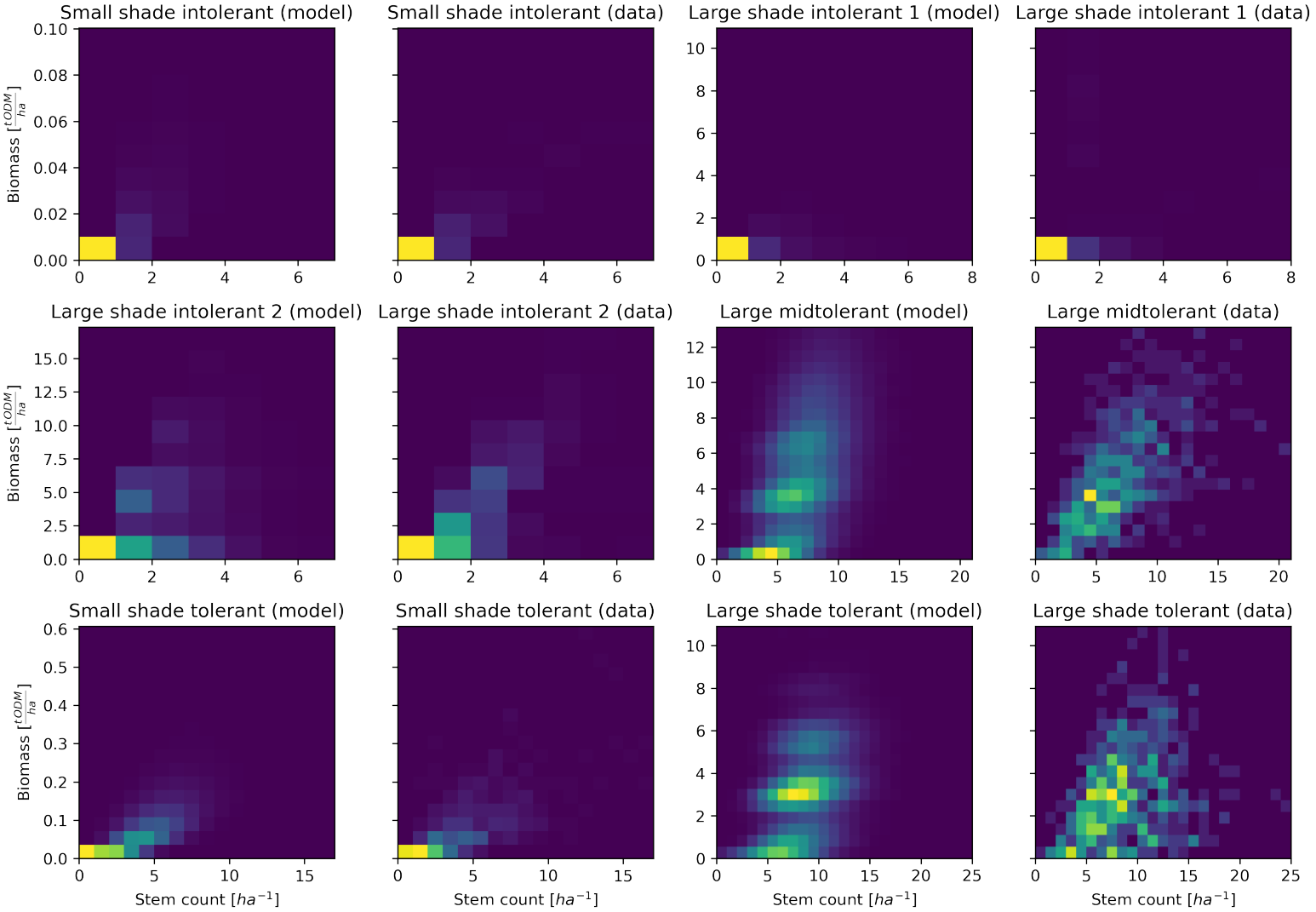

Figure S17. Comparison between model- and data-generated histograms of the joint biomass and stem count distributions for the six PFTs. Columns 1 and 3 show histograms obtained from model-generated samples; column 2 and 4 show histograms obtained from the field data. The main features of the histograms from the model and the data match, indicating a reasonable model fit.

Parameter	Unit	Optimization run	Small shade intolerant	Large shade intolerant 1	Large shade intolerant 2	Large mid-tolerant	Small shade tolerant	Large shade tolerant
$n_{\text{seeds},i}$	$\frac{1}{\text{ha}\cdot\text{yr}}$	1	1.297	9.997	1.28	4.346	2.603	3.409
		2	1.721	7.384	0.492	4.019	2.863	3.415
		3	1.288	12.061	1.358	4.367	2.941	3.318
$\theta_{\text{est},0}$	1	1	0.0714	0.202	0.0807	0.0091	0.0405	$3.36{\cdot}10^{-4}$
		2	0.0786	0.1626	0.0432	0.0066	0.0449	$1{\cdot}10^{-4}$
		3	0.0737	0.1962	0.0864	0.0116	0.048	0.002
$\theta_{\text{production},i,1}$	$\frac{\mu\text{Mol phot.}}{\text{m}^2\cdot\text{s}}$	1	500	118.56	100	70.82	274.15	492.73
		2	499.49	112.94	100	61.11	217.99	500
		3	497.23	107.87	100	61.05	245.69	401.76
γ_i	1	1	0.15	0.285	0.4	0.4	0.189	0.236
		2	0.15	0.168	0.4	0.4	0.15	0.307
		3	0.15	0.151	0.376	0.4	0.193	0.392
$q_{\Delta\text{DBH}}$	1	1	0.991					
		2	0.99					
		3	0.985					
$\theta_{\text{est},1}$	1	1	3					
		2	20					
		3	3.547					

Table S13. Parameter estimates resulting from the three optimization runs. For most of the parameters, the estimates remained in the same order of magnitude, indicating that they are estimable. Only the parameter $\theta_{\text{est},1}$ took on largely different values. This suggests that this parameter is not estimable.

S5 Variation of the CUE of mature trees

To analyze how much our results depend on the assumption that the CUE of mature trees is reduced by 100%, we considered three alternative scenarios, in which the CUE of mature trees was reduced by 50%, 25%, and 0% compared to immature trees of the same size. For each of the scenarios, we determined how the NPP depends on the covariates considered in the other parts of this paper. Note that as we assumed that a tree's maturity status does not affect its GPP, the considered scenarios would not yield different results with respect to the GPP.

The basal area of immature trees continued to be the best considered predictor, with a reasonable predictive performance ($R^2 \geq 0.53$) even when the CUE of immature trees was only reduced by 25% (Fig. S18). When the CUE was not reduced at all, the complete basal area and the basal area of immature trees had similar predictive capacity ($R^2 \approx 0.35$), and the DBH entropy became the best predictor ($R^2 = 0.4$). When the trees were weighted by their cubic diameter when computing the DBH entropy ($\eta = 3$; see section S3.2), the R^2 values remained consistently above 0.5 even when the CUE was not reduced (Fig. S19). The correspondingly adjusted DBH entropy became the best considered predictor if the CUE of mature trees was reduced by 25% or less.

These results suggest that the maturity stage of trees remains significant even if their CUE is only mildly reduced. However, the consistently high predictive capacity of the DBH entropy even in cases where mature trees did not have a reduced CUE shows that the DBH entropy captures more productivity-related forest attributes than just the fraction of mature trees.

S6 Further technical details

S6.1 Computing the weights of the tree species in the inventory

To derive allometric relationships for the different PFTs, we used data available for individual species, weighted according to their respective prevalence in the inventory. Here we describe how we computed these weights.

For every sufficiently large tree K in the forest inventory, we added one unit of weight to the data points in the allometry dataset that corresponded to trees of the same species with most similar DBH. Trees with DBH below $5\mathrm{cm}$ were ignored, as they are not considered in the model (see section S2.6). Let $\mathcal{A}$ be an index set for the allometry dataset (ignoring entries with DBH below $5\mathrm{cm}$) and s_k be the species corresponding to $k \in \mathcal{A}$. Let furthermore $\mathcal{A}_k^+ = \left\{\tilde{k} \in \mathcal{A} : \tilde{k} = s_k, d_{\tilde{k}} > d_k\right\}$ the entries in the allometry dataset that correspond to the same species and a larger DBH, and define $\mathcal{A}_k^= = \left\{\tilde{k} \in \mathcal{A} : \tilde{k} = s_k, d_{\tilde{k}} = d_k\right\}$ and $\mathcal{A}_k^- = \left\{\tilde{k} \in \mathcal{A} : \tilde{k} = s_k, d_{\tilde{k}} < d_k\right\}$ correspondingly for entries with equal or smaller DBH, respectively. Define

$$d_k^+ = \begin{cases} \min\limits_{\tilde{k} \in \mathcal{A}_k^+} d_{\tilde{k}} & \text{if } \mathcal{A}_k^+ \neq \emptyset \\ d_k & \text{else} \end{cases} \tag{S66}$$

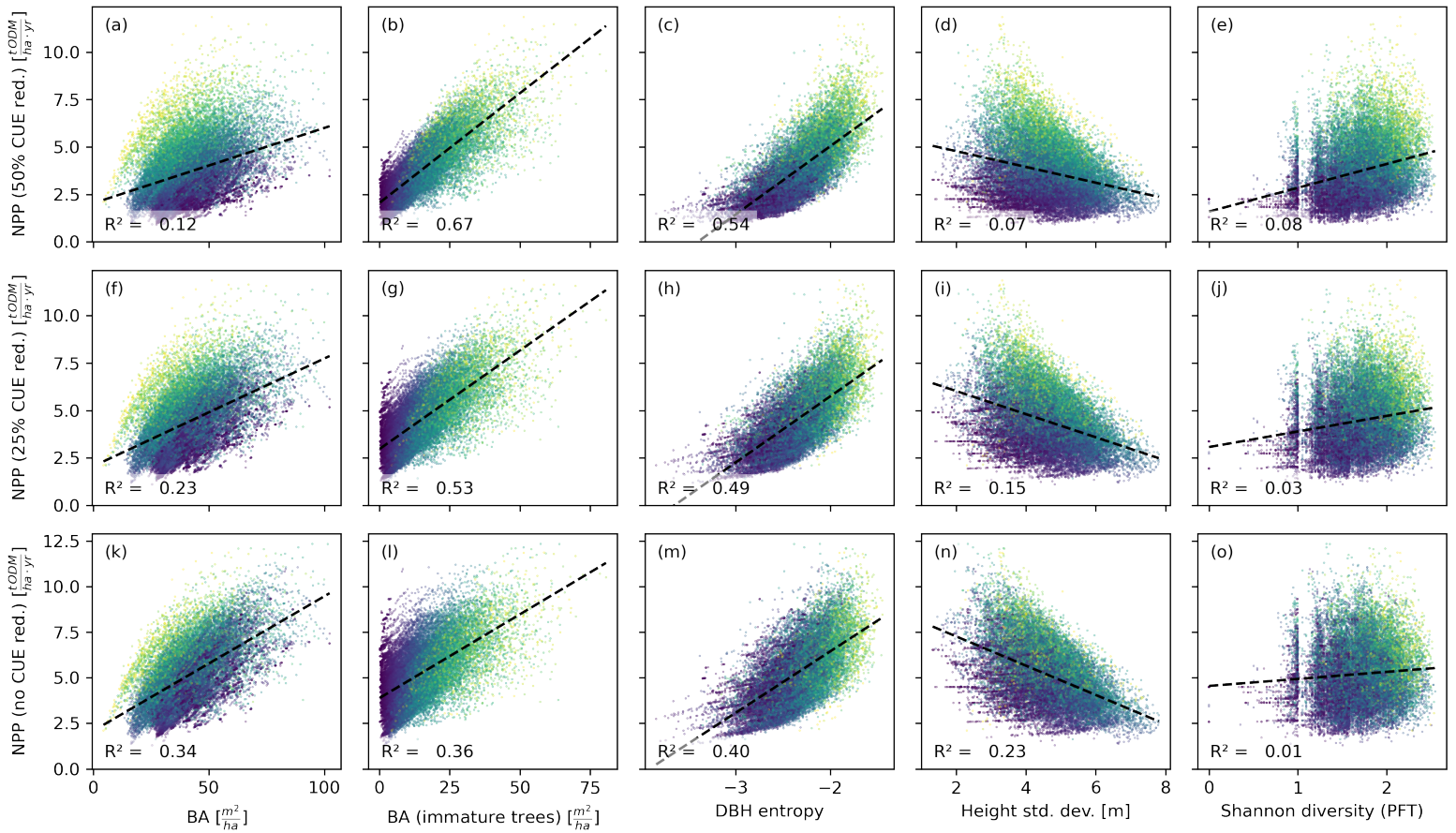

Figure S18. NPP dependent on different measures of basal area (BA) and heterogeneity for different CUE reduction scenarios. In the first row, the CUE of mature trees was only reduced by 50% as compared to immature trees of the same size; in the second row, the CUE reduction was 25%, and in the third row not existent. Each dot corresponds to a $0.04\,\mathrm{ha}$ forest patch (sample size: $25,000$). The colour indicates the basal area proportion of mature trees (blue: only mature trees; yellow: no mature trees). The basal area of immature trees remains a good predictor of NPP if the CUE is only mildly reduced for mature trees. The DBH entropy is even more robust against changes in the CUE reduction.

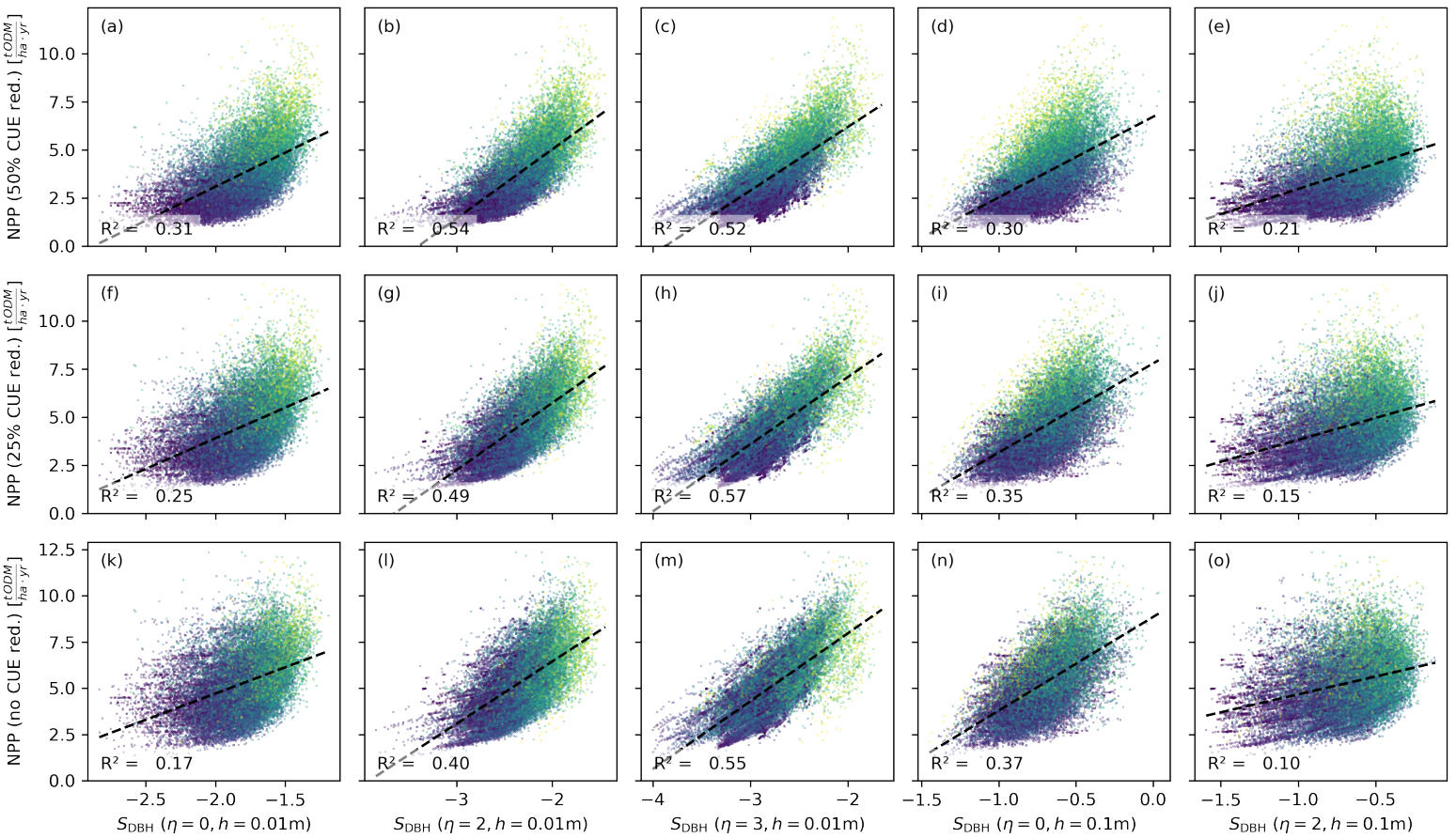

Figure S19. NPP dependent on different parameters of the DBH entropy S_{DBH} in different CUE reduction scenarios. In the first row, the CUE of mature trees was only reduced by 50% as compared to immature trees of the same size; in the second row, the CUE reduction was 25%, and in the third row not existent. Each dot corresponds to a $0.04\,\mathrm{ha}$ forest patch. The colour indicates the basal area proportion of mature trees (blue: only mature trees; yellow: no mature trees). For a CUE reduction of 50%, the relationship between DBH entropy and NPP or NEE is strongest if the DBH entropy is computed with weights based on the basal area ($\eta = 2$) and a small bandwidth $h = 1\,\mathrm{cm}$; for smaller CUE reductions, computing the weights based on the cubed DBH ($\eta = 3$) and using bandwidth $h = 1\,\mathrm{cm}$ is better and leads to a higher correlation than in any of the configurations with a CUE reduction of 50% and more.

and

$$d_k^+ = \begin{cases} \max\limits_{\tilde{k} \in \mathcal{A}_k^-} d_{\tilde{k}} & \text{if } \mathcal{A}_k^- \neq \emptyset \\ d_k & \text{else} \end{cases} \tag{S67}$$

as the smallest larger and the largest smaller DBH of an entry in the allometry dataset corresponding to the same species. The contribution v_{Kk} of tree K in the inventory to the weight of entry k in the allometry dataset is given by

$$v_{Kk} = \begin{cases} 1 & \text{if } d_K = d_k, \\ 1 & \text{if } d_K > d_k = d_{s_k}^{\max}, \\ 1 & \text{if } d_K < d_k = d_{s_k}^{\min}, \\ \frac{d_k^+ - d_K}{d_k^+ - d_k} & \text{if } d_K \in \left(d_k, d_k^+\right), \\ \frac{d_K - d_k^-}{d_k - d_k^-} & \text{if } d_K \in \left(d_k^-, d_k\right), \\ 0 & \text{else.} \end{cases} \tag{S68}$$

That is, the contribution is 1 if the diameters are equal or if the the tree diameter is outside the range of diameters covered in the allometry dataset and the allometry data entry has maximal or minimal diameter, respectively. The weights are then computed as follows:

$$w_k = c_{\text{class}(s_k)} \sum_{K \in \mathcal{I}_{s_k}} \frac{v_{\kappa k}}{|\mathcal{A}_k^=|}, \tag{S69}$$

where $c_{\text{class}(s_k)}$ is a normalization constant for the PFT $\text{class}(s_k)$ to which species s_k belongs, $\mathcal{I}_{s_k}$ is the subset of trees in the inventory that are of species s_k, and $|\cdot|$ denotes the counting norm. The division by the cardinality of $\mathcal{A}_k^=$ distributes the contribution of tree K evenly among all allometry entries with similar species and diameter. As a result, each tree in the inventory makes the same total contribution to the weights.

The normalization constants $c_{\text{class}(s_k)}$ do not affect parameter estimation, but we chose

$$c_j = \frac{|\mathcal{A}_j|}{\sum_{k \in \mathcal{A}_j} \sum_{K \in \mathcal{I}_{s_k}} \frac{v_{\kappa k}}{|\mathcal{A}_k^=|}} \tag{S70}$$

so that the sum of the weights corresponds to the size of the dataset used to fit the allometry curve for PFT j. As a result, the likelihood computed using the weights may be of the same order of magnitude as the unweighted likelihood, which can be helpful for model comparison and selection.

To compute the weights efficiently, we sorted both the allometry dataset and the inventory by tree DBH and species. Then, the weights can be computed in linear time of the inventory dataset size (assuming that there are only few entries in the allometry dataset that have both the same species and DBH).

S6.2 Assignment of new seeds to patches

Each year, a constant number of seeds is distributed evenly to the different modelled forest patches. If the provided seed number is not an integer divisible by the number of simulated patches, the seed number is rounded stochastically for each patch so that the expected number of seeds per hectare and PFT matches the provided seed number. That is, if $n_{\mathrm{seeds},i}$ is the number of seeds per hectare for PFT i and n_{patches} the number of simulated patches, then the number of seeds for a patch j is given by

$$n_{\mathrm{seeds},i,j} = \left\lfloor \frac{n_{\mathrm{seeds},i}}{n_{\mathrm{patches}}} \right\rfloor + B_{p_{\mathrm{seed}}}, \tag{S71}$$

where

$$B_{p_{\mathrm{seed}}} \sim \mathrm{Bernoulli}(p_{\mathrm{seed}}) \tag{S72}$$

is a Bernoulli distributed random variable with success probability

$$p_{\mathrm{seed}} = \frac{n_{\mathrm{seeds},i}}{n_{\mathrm{patches}}} - \left\lfloor \frac{n_{\mathrm{seeds},i}}{n_{\mathrm{patches}}} \right\rfloor. \tag{S73}$$

References

Bohn, F. J., Frank, K., and Huth, A.: Of Climate and Its Resulting Tree Growth: Simulating the Productivity of Temperate Forests, Ecological Modelling, 278, 9–17, https://doi.org/10.1016/j.ecolmodel.2014.01.021, 2014.

Cartis, C., Fiala, J., Marteau, B., and Roberts, L.: Improving the Flexibility and Robustness of Model-Based Derivative-Free Optimization Solvers, ACM Transactions on Mathematical Software, 45, 1–41, https://doi.org/10.1145/3338517, 2019.

Chojnacky, D. C., Heath, L. S., and Jenkins, J. C.: Updated Generalized Biomass Equations for North American Tree Species, Forestry, 87, 129–151, https://doi.org/10.1093/forestry/cpt053, 2014.

Conn, A. R., Gould, N. I. M., and Toint, P. L.: Trust-Region Methods, MPS-SIAM Series on Optimization, Society for Industrial and Applied Mathematics, Philadelphia, PA, 2000.

Dănescu, A., Albrecht, A. T., and Bauhus, J.: Structural Diversity Promotes Productivity of Mixed, Uneven-Aged Forests in Southwestern Germany, Oecologia, 182, 319–333, https://doi.org/10.1007/s00442-016-3623-4, 2016.

Dislich, C., Günter, S., Homeier, J., Schröder, B., and Huth, A.: Simulating Forest Dynamics of a Tropical Montane Forest in South Ecuador, ERDKUNDE, 63, 347–364, https://doi.org/10.3112/erdkunde.2009.04.05, 2009.

Fischer, R., Bohn, F., Dantas de Paula, M., Dislich, C., Groeneveld, J., Gutiérrez, A. G., Kazmierczak, M., Knapp, N., Lehmann, S., Paulick, S., Pütz, S., Rödig, E., Taubert, F., Köhler, P., and Huth, A.: Lessons Learned from Applying a Forest Gap Model to Understand Ecosystem and Carbon Dynamics of Complex Tropical Forests, Ecological Modelling, 326, 124–133, https://doi.org/10.1016/j.ecolmodel.2015.11.018, 2016.

Jones, E., Oliphant, T., and Peterson, P.: SciPy: Open Source Scientific Tools for Python, https://scipy.org/, 2001.

Liu, Q.-J.: Nested regression for establishing tree biomass equations, Chinese Journal of Plant Ecology, 33, 331, 2009.

Niinemets, Ü. and Valladares, F.: Tolerance to Shade, Drought, and Waterlogging of Temperate Northern Hemisphere Trees and Shrubs, Ecological Monographs, 76, 521–547, https://doi.org/10.1890/0012-9615(2006)076[0521:TTSDAW]2.0.CO;2, 2006.

Park, J., Kim, H. S., Jo, H. K., and Jung, I. B.: The Influence of Tree Structural and Species Diversity on Temperate Forest Productivity and Stability in Korea, Forests, 10, 1113, https://doi.org/10.3390/f10121113, 2019.

Piponiot, C., Anderson-Teixeira, K. J., Davies, S. J., Allen, D., Bourg, N. A., Burslem, D. F. R. P., Cárdenas, D., Chang-Yang, C.-H., Chuyong, G., Cordell, S., Dattaraja, H. S., Duque, Á., Ediriweera, S., Ewango, C., Ezedin, Z., Filip, J., Giardina, C. P., Howe, R., Hsieh, C.-F., Hubbell, S. P., Inman-Narahari, F. M., Itoh, A., Janík, D., Kenfack, D., Král, K., Lutz, J. A., Makana, J.-R., McMahon, S. M., McShea, W., Mi, X., Bt. Mohamad, M., Novotný, V., O'Brien, M. J., Ostertag, R., Parker, G., Pérez, R., Ren, H., Reynolds, G., Md Sabri, M. D., Sack, L., Shringi, A., Su, S.-H., Sukumar, R., Sun, I.-F., Suresh, H. S., Thomas, D. W., Thompson, J., Uriarte, M., Vandermeer, J., Wang, Y., Ware, I. M., Weiblen, G. D., Whitfeld, T. J. S., Wolf, A., Yao, T. L., Yu, M., Yuan, Z., Zimmerman, J. K., Zuleta, D., and Muller-Landau, H. C.: Distribution of Biomass Dynamics in Relation to Tree Size in Forests across the World, New Phytologist, 234, 1664–1677, https://doi.org/10.1111/nph.17995, 2022.

Silva Pedro, M., Rammer, W., and Seidl, R.: Disentangling the Effects of Compositional and Structural Diversity on Forest Productivity, Journal of Vegetation Science, 28, 649–658, https://doi.org/10.1111/jvs.12505, 2017.

Sun, R., Chen, J. M., Zhu, Q., Zhou, Y., Liu, J., Li, J., Liu, S., Yan, G., and Tang, S.: Spatial Distribution of Net Primary Productivity and Evapotranspiration in Changbaishan Natural Reserve, China, Using Landsat ETM+ Data, Canadian Journal of Remote Sensing, 30, 731–742, https://doi.org/10.5589/m04-040, 2004.

Varin, C.: On Composite Marginal Likelihoods, AStA Advances in Statistical Analysis, 92, 1–28, https://doi.org/10.1007/s10182-008-0060-7, 2008.

Wales, D. J. and Doye, J. P. K.: Global Optimization by Basin-hopping and the Lowest Energy Structures of Lennard-Jones Clusters Containing up to 110 Atoms, The Journal of Physical Chemistry A, 101, 5111–5116, https://doi.org/10.1021/jp970984n, 1997.

Wand, M. P. and Jones, M. C.: Kernel Smoothing, no. 60 in Monographs on Statistics and Applied Probability, Chapman & Hall, London ; New York, 1st ed edn., 1995.

Wang, H., Xu, J., Sheng, L., Ma, L., and Liu, X.: Study on the Characteristics of Climate Change in Changbai Mountain National Natural Reserve from 1958 to 2017, Arabian Journal of Geosciences, 13, 777, https://doi.org/10.1007/s12517-020-05808-7, 2020.

Wang, X., Ye, J., Li, B., Zhang, J., Lin, F., and Hao, Z.: Spatial Distributions of Species in an Old-Growth Temperate Forest, Northeastern China, Canadian Journal of Forest Research, 40, 1011–1019, https://doi.org/10.1139/X10-056, 2010.

Weedon, G. P., Balsamo, G., Bellouin, N., Gomes, S., Best, M. J., and Viterbo, P.: The WFDEI Meteorological Forcing Data Set: WATCH Forcing Data Methodology Applied to ERA-Interim Reanalysis Data, Water Resources Research, 50, 7505–7514, https://doi.org/10.1002/2014WR015638, 2014.

West, G. B., Brown, J. H., and Enquist, B. J.: A General Model for the Structure and Allometry of Plant Vascular Systems, Nature, 400, 664–667, https://doi.org/10.1038/23251, 1999.

Xu, Z., Liu, Q., Du, W., Zhou, G., Qin, L., and Sun, Z.: Modelling Leaf Phenology of Some Trees with Accumulated Temperature in a Temperate Forest in Northeast China, Forest Ecology and Management, 489, 119 085, https://doi.org/10.1016/j.foreco.2021.119085, 2021.